

1 Small emission sources **in aggregate** disproportionately account 2 for a large majority of total methane emissions from the US oil 3 and gas sector

4 James P. Williams¹, Mark Omara^{1,2}, Anthony Himmelberger², Daniel Zavala-Araiza¹, Katlyn
5 MacKay¹, Joshua Benmergui^{1,2,3}, Maryann Sargent³, Steven C. Wofsy³, Steven P. Hamburg^{1,2},
6 Ritesh Gautam^{1,2}

7 ¹Environmental Defense Fund, New York, NY, USA 10010

8 ²MethaneSAT, LLC, Austin, TX, USA 78701

9 ³Harvard University, Cambridge, MA, USA 02138

10
11 Correspondence to: James P. Williams (jamwilliams@edf.org), Ritesh Gautam (rgautam@edf.org)
12

13
14 **Abstract.** Reducing methane emissions from the oil and gas (oil/gas) sector has been identified as a critically
15 important global strategy for reducing near-term climate warming. Recent measurements, especially by satellite and
16 aerial remote sensing, underscore the importance of targeting the small number of facilities emitting methane at high
17 rates (i.e., “super-emitters”) for measurement and mitigation. However, the contributions from individual oil/gas
18 facilities emitting at low emission rates that are often undetected are poorly understood, especially in the context of
19 total national- and regional-level estimates. In this work, we compile empirical measurements gathered using
20 methods with low limits of detection to develop a facility-level model to quantify estimates of total methane
21 emissions from the continental United States (CONUS) midstream and upstream oil/gas sector for 2021. We find
22 that ~70% (95% confidence intervals: 63-82/61-81%) of the total 14.6 (12.7-16.8) Tg/yr oil/gas methane emissions
23 in the CONUS for the year 2021 (Total: 14.3 Tg/yr) originate from facilities emitting <100 kg/hr, and 30% (26-
24 34%) and ~80% (68-90%) from facilities emitting <10 kg/hr and <200 kg/hr, respectively. While there is variability
25 among the emission distribution curves for different oil/gas production basins, facilities with low emissions are
26 consistently found to account for the majority of total basin emissions (i.e., range across basins 63%–90 of 60% -
27 86% of total basin emissions from facilities emitting <100 kg/hr). Production We estimate that production well sites
28 were responsible for 70% of total regional oil/gas methane emissions, with from which we find the highest
29 contributions from a large population of low-producing well sites that accounted for only 10% of national oil and
30 gas production in 2021, disproportionately accounted for 77% (72-81%) of the total well site emissions. Our results
31 are also in broad agreement with data obtained from several independent aerial remote sensing campaigns (e.g.,
32 MethaneAIR, Bridger Gas Mapping LiDAR, AVIRIS-NG, and Global Airborne Observatory) across 5-8 major
33 oil/gas basins. Our findings highlight the importance of accounting for the significant contribution of small emission
34 sources to total oil/gas methane emissions. While reducing emissions from high-emitting facilities is important, it is
35 not sufficient for the overall mitigation of methane emissions from the oil and gas sector which according to this
36 study is dominated by small emission sources across the US. Tracking changes in emissions over time and designing
37 effective mitigation policies should consider the large contribution of small methane sources to total emissions.

38

39

40 1 Introduction

41

42 Methane is a short-lived but powerful greenhouse gas with a global warming potential more than 80 times
43 stronger than carbon dioxide (CO₂) over 20 years (AR6 Synthesis Report: Climate Change 2023, 2024). Therefore,
44 the reduction of methane emissions has become a key goal to achieve rapid climate mitigation in the short term
45 (Ocko et al., 2021). In North America, one of the largest sources of methane emissions originates from the oil and
46 gas (oil/gas) sector, with most emissions originating from the production (i.e., upstream) and transportation/storage
47 (i.e., midstream) sectors (Alvarez et al., 2018). Multiple studies, especially over the past decade, have focused on the
48 quantification of methane sources from the oil/gas sector, with particular emphasis on the continental United States
49 (CONUS) (Alvarez et al., 2018; de Gouw et al., 2020; Omara et al., 2018; Lu et al., 2022; Zhang et al., 2020; Shen
50 et al., 2022; Cusworth et al., 2022; Nesser et al., 2023; Brandt et al., 2016; Duren et al., 2019; Maasakkers et al.,
51 2021; Lu et al., 2023; Worden et al., 2022). Several studies have recognized the importance of a small percentage of
52 high-emitting sites (i.e. “super-emitters”) and reported them as accounting for a large fraction of total methane
53 emissions (Brandt et al., 2016; Cusworth et al., 2022; Duren et al., 2019; Sherwin et al., 2024). The emission rate
54 thresholds that characterize these super-emitting facilities are critical information for methane measurement
55 platforms, especially remote sensing technologies focused on detecting high-emitting point sources. Aerial and
56 satellite remote sensing technologies have enabled more frequent monitoring of emissions from oil and gas sites and
57 rapid mapping of large areas, although they face limitations in detection sensitivity. Despite the improved ability to
58 locate and quantify emissions from high-emitting sites, there has been considerable lack of understanding about the
59 characteristics of low methane emitting facilities, especially those emitting at rates below the limits of detection
60 (LOD) of most point-source detection remote sensing platforms, and their contributions to total oil/gas methane
61 emissions.

62 While some studies offer important yet limited insights into the contributions of different lower-emitting
63 infrastructure from the CONUS oil/gas sector, there is a lack of understanding about their overall contribution to the
64 total sectoral regional and national scale emissions. A recent study by Xia et al. (2024) combined aerial remote
65 sensing data from Bridger Gas Mapping LiDAR (Bridger GML) in four oil/gas basins supplemented with
66 component-level modeling for facilities emitting below the Bridger GML LOD and found significantly more
67 emission sources in the 1 – 10 kg/hr range when compared to the emission distribution used by the EPA (Xia et al.,
68 2024). In a study focused on production well sites in the CONUS, the main source of methane emissions from the
69 oil/gas sector (Alvarez et al., 2018; Omara et al., 2018; Rutherford et al., 2021), Omara et al. (2018) found that 90%
70 of total methane emissions from producing well sites came from those emitting at rates <100 kg/hr. A follow-up
71 study by Omara et al. (2022) highlights that the total methane emissions from low-producing well sites producing

72 less than 15 boe/day (i.e., 1 Mcf = 1,000 cubic feet of natural gas = 19.2 kg of methane at 15.6 °C and 1 atmosphere;
73 1 boe = 1 barrel of oil equivalent = 6 Mcf; **assumed methane content in natural gas of 80%**), which comprise 80% of
74 all producing well sites in the CONUS, were responsible for nearly half of all methane emissions from the oil/gas
75 production sector. Kunkel et al. (2023) observed that the use of the Bridger GML remote sensing platform with an
76 LOD of 3 kg/hr, combined with prior Carbon Mapper detections in a section of the Permian basin showed a
77 significant contribution from sources below the listed LOD of Carbon Mapper of 10 kg/hr. Cusworth et al. (2022)
78 found that 35% of total methane emissions (including non-oil/gas sources) from several major oil/gas producing
79 basins (other than the Appalachian basin) in the CONUS come from facilities emitting >10 kg/hr, indicating that
80 65% of emissions come from facilities emitting <10 kg/hr. Although these studies using independent measurement
81 platforms provide new emerging insights about the importance of low methane emitting oil/gas facilities, there
82 generally remains a lack of quantitative assessment of the relative fractions of emissions originating from different
83 emission rate thresholds aggregated over individual oil/gas basins as well as at a national scale.

84 There are a variety of different methane quantification methods that differ in terms of their spatial resolution of
85 sources, logistical constraints, costs of implementation, and their LODs. Measurement method sensitivities and
86 LODs have important policy implications. For example, the Environmental Protection Agency (EPA) recently
87 finalized regulations that define a “super-emitter event” as an emission rate threshold of 100 kg/hr or greater
88 (Standards of Performance for New, Reconstructed, and Modified Sources and Emissions Guidelines for Existing
89 Sources: Oil and Natural Gas Sector Climate Review, 2024), albeit without clear information on what percentage of
90 total regional emissions are captured within this definition. Satellite and aerial remote sensing methods have point
91 source LODs that range anywhere from 1-3 kg/hr for Bridger’s airborne GML (Johnson et al., 2021; Kunkel et al.,
92 2023; Thorpe et al., 2024; Xia et al., 2024) to ~200 kg/hr for GHGSat (Sherwin et al., 2023). In contrast, ground-
93 based measurement methods such as OTM-33a and tracer release have LODs <1 kg/hr (Fox et al., 2019). A study by
94 Ravikumar et al. (2018) using the Fugitive Emissions Abatement Simulation Toolkit (FEAST) suggests that a
95 method with a LOD of 0.1-1 kg/hr would sufficiently capture all emissions from the oil/gas sector, whereas the
96 ability to quantify emissions below this threshold would not lead to any significant increases in mitigation.
97 Ultimately, there is a need for clarification in the total percentage contribution of emissions originating from a given
98 emission rate threshold, which requires characterizing entire emissions distributions, not only the high emitters.

99 In this work, we create and analyze measurement-based methane emission rate distributions of US upstream and
100 midstream oil/gas facilities to determine the percentage contributions of different emission rate thresholds to total
101 methane emissions. First, we use empirical measurements gathered from ground-based sampling platforms to
102 develop a bottom-up facility-based model to estimate methane emissions for upstream and midstream facilities in
103 the continental US (CONUS) for 2021. Next, we aggregate our facility-level, population-based data to determine the
104 national- and basin-level contributions of methane emissions originating from facilities emitting at different
105 emission rate thresholds, in addition to comparisons to aerial-remote sensing platforms. Finally, we break down the
106 emission distribution curves by facility category to analyze how the percentage contributions of total emissions vary
107 across facility types.

108

109 2 Materials and methods

110

111 2.1 Empirical measurements

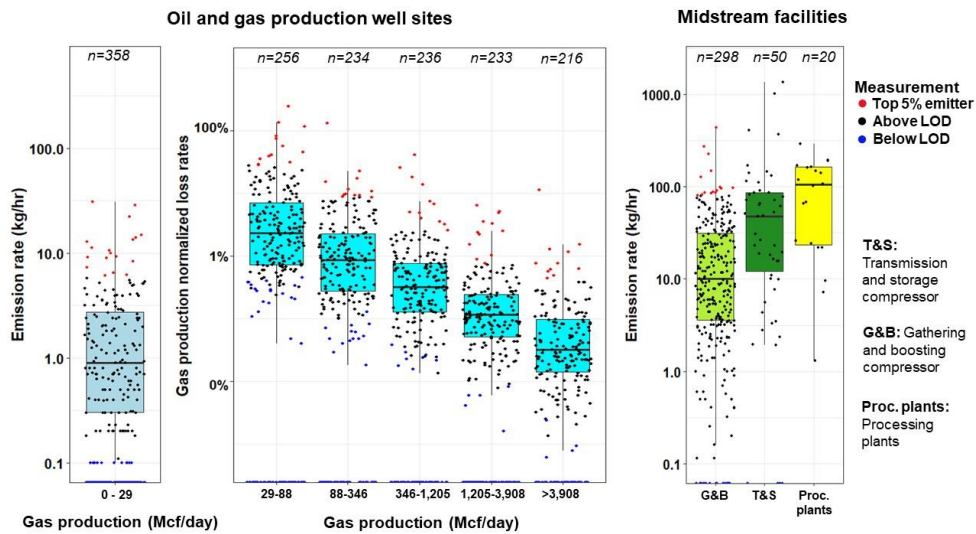
112

113 We compile 1,901 facility-level methane emission rate measurements from 16 studies (Brantley et al., 2014;
114 Caulton et al., 2019; Deighton et al., 2020; Goetz et al., 2015; Lan et al., 2015; Mitchell et al., 2015; Omara et al.,
115 2016, 2018; Rella et al., 2015; Riddick et al., 2019; Robertson et al., 2017, 2020; Subramanian et al., 2015;
116 Yacovitch et al., 2015; Zhou et al., 2021; Zimmerle et al., 2020) that use ground-based site/facility level and
117 source/component level measurement methods with low LOD's of ~0.1 kg/hr. Most (i.e., 85%) of empirical
118 measurements we use in this work were gathered using ground-based mobile laboratories that quantified methane
119 emissions at the site/facility level using either tracer-based releases, the EPA Other Test Method (OTM-33a), or
120 Gaussian plume transport modeling (Fox et al., 2019) (Table S2). The remaining 15% of empirical measurements we
121 use (Deighton et al., 2020; Riddick et al., 2019; Zimmerle et al., 2020) are ground-based methods that aggregated
122 source/component-level HiFlow sampling or static/dynamic chamber measurements, which could mean that other
123 on-site emission sources were not quantified during measurement and overall emission rate estimates are
124 conservative.

125 The compiled empirical measurements target a variety of production well sites and/or midstream facilities
126 across at least nine oil/gas-producing basins in the CONUS (Table S2S3). For all facility categories (i.e., [production](#)
127 [well sites](#), [gathering and boosting](#) compressor stations, [transmission and storage compressor stations](#), and [processing](#)
128 [plants](#), ~~[production well sites](#)~~), we prioritize datasets of randomly sampled sites that include measurements below the
129 method's LOD or reported as zero emissions, except for measurements from two studies ([Brantley et al., 2014](#); [Lan](#)
130 [et al., 2015](#)) ([Brantley et al., 2014](#); [Lan et al., 2015](#)) which we discuss later in Section 2.3. Additionally, for
131 production well site measurements, we focus only on data that provide facility-level gas production data for the
132 date/month of measurement. Our compiled dataset of measurements includes both routine intentional (e.g., venting
133 from pneumatic devices) and non-intentional (e.g., malfunctioning equipment [and/or leaks from valves, connectors,](#)
134 [flanges, etc](#)) emissions, and while we remove any measurements attributed to high emitting intermittent events such
135 as flowbacks and liquids unloadings if that information is present, we cannot fully discount that emissions from
136 these high-emitting intermittent [sources](#) are included in our compiled dataset. Furthermore, we remove any
137 empirical measurement data associated with flaring emissions, which are [treated separately as](#) discussed below, if
138 that information is provided in the empirical data.

139 We categorize the empirical measurements by facility category as production well sites, gathering and boosting
140 compressor stations (G&B compressors), transmission and storage compressor stations (T&S compressors), or
141 processing plants. We group the empirical measurements from production well sites into six production bins based
142 on gross average daily gas production as reported in individual studies. We use gross daily average gas production

143 data instead of oil and gas production data for two reasons: 1) the limited availability of facility-level oil production
 144 data provided from empirical ~~measurements~~ measurement studies; and 2) the established relationship between gas
 145 production and emission rates observed in previous work (Omara et al., 2018, 2022, 2024a) (Omara et al., 2018,
 146 2022, 2024). The gas production ranges of the production bins (Fig. 1) are chosen to evenly distribute empirical
 147 measurements above the method LOD to all six production bins. This categorization creates nine distinct facility
 148 categories: G&B compressors, T&S compressors, processing plants, and six groups of production well sites. We
 149 further classify the nine distinct facility categories into five primary facility categories: low-production well sites
 150 which produce combined oil and gas <15 boedboe/day (i.e., 0.13 kt of methane production per year), non-low-
 151 producing well sites which produce ≥15 boedboe/day, processing plants, G&B compressors, and T&S compressors.
 152 In addition to these facility categorizations, we also include Visible Infrared Imaging Radiometer Suite (VIIRS)
 153 flare detections and flared gas volume estimates in our analysis, which are treated as an independent methane source
 154 since flares can be located on multiple facility categories across the upstream and midstream oil/gas sectors.



155
 156 **Figure 1:** Facility-level empirical measurement data distributed by different distinct facility categories for production well sites
 157 (left) and midstream facilities (right). Individual measurements are shown for each box plot and colored according to their
 158 emission rate status for that facility category, where blue points are considered non-detectable emissions below an emission rate
 159 threshold of ≤0.1 kg/hr/facility which is the method LOD we use, black points are measurements above our method LOD but
 160 below the top 5% emitter category, and red points are the top 5% of empirical emission rates for that facility category. The
 161 number of empirical measurements available for each facility category is denoted at the top of each boxplot. We show emission
 162 rates rather than loss rates for the lowest cohort of production well sites due to the reasoning presented in Section 2.3. Unit
 163 conversions: 1 Mcf = 1,000 cubic feet of natural gas = 19.2 kg of methane at 15.6 °C and 1 atmosphere; 1 boe = 1 barrel of oil
 164 equivalent = 6 Mcf; assumed methane content in natural gas of 80%.

165 Mcfd — thousands of cubic feet of gas per day, Proc. Plants — processing plants, G&B — gathering and boosting compressor station, T&S —
 166 transmission and storage compressor station, LOD — limit of detection.

167
168
169

2.2 Activity data

170 We use activity data (i.e., number of facilities and spatial locations) for actively producing wells in 2021
171 provided by Enverus for the CONUS. We calculate both the annual averaged daily gross gas production, and oil and
172 gas production for each producing well using the number of producing days and total annual oil and gas production
173 data provided by Enverus. We convert production wells to production well sites by spatially aggregating individual
174 wells within 25-meter (vertical wells) or 50-meter (horizontal wells) distances from each other and ~~merging their~~
175 ~~combined oil and gas production in boed and gas production in thousand cubic feet per day (Mcf), similar to~~
176 ~~previous approaches (Omara et al., 2018); separately merging their combined oil and gas production and gas~~
177 ~~production, and converting these production values to a mass equivalent production rate in kg/hr of methane (i.e., 1~~
178 ~~Mcf = 1,000 cubic feet of natural gas = 19.2 kg of methane at 15.6 °C and 1 atmosphere; 1 boe = 1 barrel of oil~~
179 ~~equivalent = 6 Mcf; assumed methane content in natural gas of 80%), similar to previous approaches (Omara et al.,~~
180 ~~2018).~~

181 We acquire activity data for operational transmission and storage (T&S) and gathering and boosting (G&B)
182 compressor stations and processing plants from Enverus for 2021 for the CONUS, which was further supplemented
183 by additional data from the Oil and Gas Infrastructure Mapping (OGIM) database published in Omara et al. (2023).
184 We filter data for these midstream facilities to include only active facilities in the year 2021. For VIIRS flare
185 detections, we use the 2021 natural gas flared volume estimates (Elvidge et al., 2016) based on natural gas flaring
186 detections provided by the VIIRS instruments installed aboard satellite platforms which have a 750x750 meter
187 source resolution (NOAA-20 and Suomi National Polar-orbiting Partnership) (Elvidge et al., 2017); (Elvidge et al.,
188 2015). In terms of potential double-counting between the VIIRS flare detections and the empirical measurements we
189 use in this work, the majority of VIIRS detections are in the Permian, Bakken, and Eagle Ford oil/gas basins (i.e.,
190 86% of total VIIRS detections) which corresponds to a small number of our empirical measurement data (Table S2)
191 (Plant et al., 2022; S3) (Plant et al., 2022). However, the limited availability of spatial coordinates for our empirical
192 measurements restricts our ability to perform a direct comparison to exclude overlapping/proximal VIIRS detections
193 and our facility-level empirical measurements. Therefore, we do acknowledge that there is a possibility of double
194 counting between our empirical measurement data and the VIIRS flare detections, but we expect the degree of
195 overlap to be low.

2.3 Facility-level methane emission inventory

197 We calculate annual methane emissions from all facility categories (i.e., six production bins of production well
198 sites, T&S compressor stations, G&B compressor stations, ~~and~~ processing plants, ~~and~~ VIIRS flare detections) using
199 a multi-step probabilistic modeling approach adapted from multiple studies (Omara et al., 2018, 2022; Plant et al.,
200 2022) (Fig. 2). Briefly, for each individual facility and VIIRS flare detection in the CONUS for 2021, we estimate an
201 annually averaged methane emission rate using empirical measurement data, and consequently the cumulative
202 distribution of methane emission rates from the aggregation of these individual emission rates. Each emission rate

estimate is indexed according to the corresponding replicate (n=500), and we use these repetitions to determine uncertainty for the cumulative methane emission distribution curves. The detailed steps of this process for all facility categories and VIIRS flare detections are described below.

For the highest five gas production bins of producing well sites ranging from 27–29 to >3,864 Mcf/day (or 4.5–644 boed to >27 kt of methane production per year, Figure 1), we use gross gas production normalized loss rates to model the distributions used to calculate methane emission rates from Eq. (1), where the Loss rate is the fraction of emitted gas relative to gas production, σ_{CH_4} is the methane content of the emitted gas (i.e., which we assume to be 80%), and $\rho(CH_4)$ is the density of methane at 15°C and 101.325 kPa (1 Mcf = 1,000 cubic feet of natural gas = 19.2 kg/m³ of methane at 15.6 °C and 1 atmosphere; 1 boe = 1 barrel of oil equivalent = 6 Mcf). For the lowest well site gas production bin of 0 to 29 Mcf/day (i.e., 0–27 Mcf to 0.2 kt of methane production per year) and midstream facilities, we use the empirical absolute methane emission rate data as is. This approach is partly based on the methods used by Omara et al. (2020) for the non-low production well site category, which exploits a weak relationship between gross gas production data (which is most accessible in empirical measurement studies) and absolute emission rates to better extrapolate emissions to the entire population of production well sites in the CONUS.

$$Emission\ rate\ \left[\frac{kg}{hr}\right] = Loss\ rate \times Gas\ production\ \left[\frac{Mcf}{day}\right] \times \frac{1000\ [cf^3]}{1\ [Mcf]} \times \frac{1\ [day]}{24\ [hr]} \times CH_4 \times \frac{0.0283\ [m^3]}{1\ [cf^3]} \times \rho(CH_4) \quad (1)$$

$$Loss\ rate = \frac{Emission\ rate\ \left[\frac{kg}{hr}\right]}{\sigma_{CH_4} \times Gas\ production\ \left[\frac{kg}{hr}\right]} \quad (1)$$

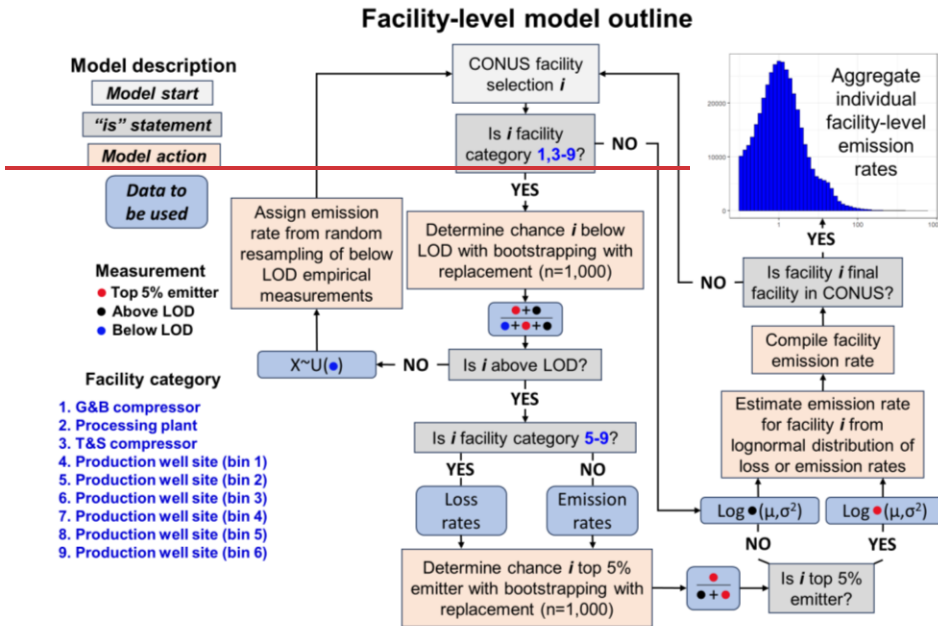
For our estimation of facility-level emission rates, we break down the modeling process into two separate steps: the first determines whether a randomly selected facility is emitting methane above our method LOD of ≤0.1 kg/hr/facility, and the second determines the associated methane emission rate for that individual facility. To test the sensitivity of our method to the selection of the method LOD, we also perform an additional sensitivity analysis for other method LODs (Fig. S11–S13). The processes outlined below are all specific to each of our nine facility categories. Measurements from Brantley et al. (2014) and Lan et al. (2015) are excluded from this first step since they do not include measurements below the method LOD but do include valuable data on well site emission rates with associated well site production data. To determine whether a facility is emitting methane above the method LOD threshold in our estimates, we first use bootstrapping with replacement (n=1,000) of our empirical measurement data to determine the chance of an individual facility emitting methane above the method LOD (i.e., ≤0.1 kg/hr/facility), which we call an “emitting facility” or “emitter” herein (Fig. 2). We model the results of the bootstrapping with replacement as a normal distribution and use the parameters of the modeled distribution to randomly determine whether a facility is emitting. Next, we remove the empirical measurements below the LOD and use bootstrapping with replacement (n=1,000) on the above LOD empirical measurements to determine the

236 probability of an emitting facility being in the top 5% (i.e., 95th percentile or above of empirical measurement data)
237 or bottom 95% (i.e., 95th percentile or below the empirical measurement data) of emitters, except for processing
238 plants and T&S compressors which had too few measurements (n=20 and n=50 respectively) to distinguish between
239 the top 5% and bottom 95% of emission or loss rates. This pseudo-random selection of a top 5% emitter within each
240 facility category accounts for the functional definition of abnormally large emissions (i.e., super-emitters) that can
241 be observed in all facility categories (including well sites in different production bins) (Zavala-Araiza et al. 2015,
242 Brandt et al. 2016). We fit the results of the bootstrapping to two normal distributions: one for the top 5% of emitters
243 and one for the bottom 95% of emitters. We use the associated parameters of each normal distribution to randomly
244 determine whether a facility is emitting in the top 5% or bottom 95% of emitters. These steps are repeated for each
245 facility for each facility category in the CONUS.

246 At the end of the first step of this facility-level modeling process, all facilities in the CONUS are classified as
247 either a: bottom 95% emitter, top 5% emitter, or below the method LOD. For facilities classified as the top 5% and
248 bottom 95% of emitters, we estimate their methane emissions by first fitting a lognormal distribution to the
249 empirical measurement data, including measurements from Brantley et al. (2014) and Lan et al. (2015), of either the
250 gas production normalized loss rates or methane emission rates (Eq. 1), depending on the facility category. Next, we
251 use the parameters of the modeled distributions to randomly assign either an emission or loss rate to a randomly
252 selected facility (n=500), depending on its emitter status and facility category. We test each estimated methane
253 emission distribution to the associated empirical measurements and find a good fit for all facility categories (Table
254 S5S6). To account for facilities emitting below the method LOD, we randomly assign an emission rate from re-
255 sampling our dataset of empirical measurements below the method LOD for that facility category. Finally, once all
256 facilities are assigned an emission rate, we compile the ensemble of emission distributions to develop facility-level
257 emission distribution curves and total regional oil/gas methane emissions for the CONUS in 2021.

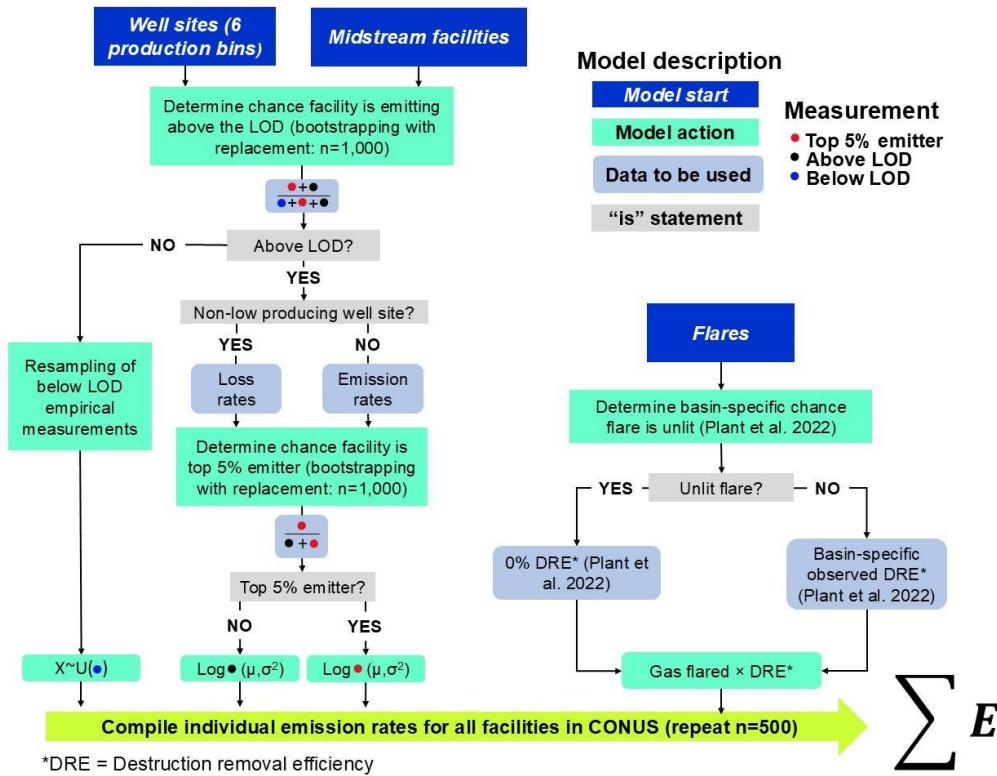
258 For all VIIRS flares detections, we use the total reported volumes of gas flared for 2021 ~~by from flares detected~~
259 using the VIIRS instrument (Elvidge et al. ~~(2016)~~2015) multiplied by the ~~flaring combustion~~observed flare
260 destruction efficiencies and percentage of unlit flares from Plant et al. (2022) to calculate annual methane emission
261 rates from this source. As previously stated, our empirical measurements are largely located outside of oil/gas basins
262 ~~(i.e. Permian, Eagle Ford, and Bakken)~~ where the majority of VIIRS flare detections are located, ~~(i.e. Permian, Eagle~~
263 Ford, and Bakken), but we cannot discount the possibility that there are instances of double-counting flares
264 measured via our ground-based empirical data and those detected by VIIRS. ~~We model flaring combustion~~For each
265 VIIRS flare detection, we randomly determine whether it is an unlit or lit flare based on the basin-specific
266 percentages of unlit flares reported by Plant et al. (2022). If a flare is determined to be lit, we use the corresponding
267 basin-specific observed destruction removal efficiencies as reported by Plant et al. (2022) multiplied by the
268 corresponding annual total volume of gas flared and convert to an emission rate. The basin-specific observed
269 destruction removal efficiencies are estimated through a fitted normal distribution using the probability distribution
270 parameters for the mean and standard deviations modeled from the 95% confidence intervals presented in Plant et al.
271 (2022). If a flare is determined to be unlit, we use a destruction removal efficiency of 0%. For VIIRS flare detections

272 located outside of the Bakken, Eagle Ford, and Permian basins (Plant et al., 2022). For areas outside of these basins,
 273 we used the total CONUS averaged flaring efficiencies destruction removal efficiencies of 95.2% (95% confidence
 274 interval: 94.3 – 95.9%) and percentage of unlit flares of 4.1% as reported by Plant et al. (2022) of 91.1% (95%
 275 confidence interval: 90.2 – 91.8%)(2022).



276

277



278

279 **Figure 2:** Flowchart of describing the facility-level estimates, with steps colored according to the specific process and data being
 280 used. The methods used for estimating methane emissions from VIIRS flare detections are not shown here but are
 281 presented in the Methods section. We note that methane emission rates for flares are calculated using a separate approach from
 282 that of production well sites and midstream facilities. Processing plants and T&S compressors are excluded from the
 283 determination of whether a facility is a top 5% emitter due to a lack of available empirical measurement data.

284

285 **2.4 Extrapolation to smaller spatial boundaries**

286

287 We perform several comparisons of our estimated emission distribution curves and total aggregated
 288 emissions to estimates from aerial and satellite remote-sensing studies. For comparisons to satellite remote-sensing
 289 studies, we prioritize national-level satellite inversions that estimate methane emissions from the CONUS that
 290 include spatially explicit maps of methane emission inversions specifically for oil/gas sources. We join the spatially
 291 explicit satellite inversions of methane emissions to the top twelve producing oil/gas basin boundaries in the
 292 CONUS, in addition to their national-level inversions which we also use for national comparisons. Since our
 293 facility-level model includes geo-located activity data (i.e., facility coordinates), we can estimate facility-level

294 methane emissions distributions and estimate total methane emissions for any spatial boundary in the CONUS by
295 spatially joining facilities within a target boundary. Spatial variability in our facility-level estimates is driven by two
296 main factors: counts of facilities and facility types, and averaged annual production characteristics. Due to
297 constraints on data availability, we do not constrain our available empirical measurement data to the specific regions
298 where they were gathered (Table S2S3). We ~~do note that basin-to-basin comparison tested the sensitivity of~~
299 ~~the excluding~~ empirical measurement data for production well sites that we use in this work generally do not
300 ~~show measurements gathered from specific oil/gas on the national emission distribution curves and total national~~
301 ~~methane emissions and found no~~ significant variations throughout the well-site production bins, with some
302 ~~exceptions variation~~ (Fig. S3-S8S9). Due to a lack of data availability, we do not have sufficient spatial information
303 from empirical measurements of G&B compressors, T&S compressors, and processing plants to test for basin-level
304 differences in empirical measurement data.

305 For comparisons to aerial remote sensing studies/results, we prioritize studies that include both measured
306 point sources (i.e., oil/gas methane sources that are above the LOD of the aerial remote sensing measurement
307 platform), estimates of total regional oil/gas emissions, and descriptions/outlines of the surveyed spatial domains
308 which are required for these comparisons. Based on these criteria, we compare our estimated emissions to those
309 from peer-reviewed studies (Cusworth et al., 2022; Kunkel et al., 2023; Xia et al., 2024) and the results of research
310 flights from MethaneAIR in the Permian and Uinta oil/gas basins (Omara et al., 2024; Chan Miller et al., 2023;
311 Chulakadabba et al., 2023; MethaneAIR, 2024), with discussion in later sections on a recent study by Sherwin et al.
312 (2024). In all cases, we estimate facility-level methane emissions within the spatial domains outlined by the aerial
313 remote sensing studies to estimate region-specific methane emission distribution curves, ~~use the relevant method~~
314 ~~limits of detection to characterize emission rate thresholds valid for comparison, and subtract any emission unrelated~~
315 ~~to the facility types we characterize (Chen et al., 2024). In the case of Cusworth et al. 2022, we infer the spatial~~
316 ~~domains by georeferencing figures from their studies using the georeferencer tool QGIS (v.3.34.2-Prizen).~~ We
317 compare our ~~spatially joined~~ spatially joined facility-level emission distributions to the percentage of emissions
318 contributed from facilities emitting below discrete methane emission rate thresholds for all four aerial remote
319 sensing studies, and to the continuous cumulative methane emissions distribution curves from Bridger GML surveys
320 (Kunkel et al., 2023; Xia et al., 2024).

321 Each aerial remote sensing campaign utilizes independent methods to estimate their percentage
322 contributions from small methane sources, which in some cases requires additional analysis of the aerial remote
323 sensing results. For our analysis of continuous methane emissions distribution curves from the Bridger GML
324 campaigns (Kunkel et al., 2023; Xia et al., 2024), we restrict our analysis to estimated emission rates >3 kg/hr,
325 which is the approximate LOD of the Bridger GML remote sensing platform. For MethaneAIR, we use the
326 percentage of area emissions (i.e., diffuse area methane sources) relative to the total methane emissions for the
327 spatial boundary, which roughly corresponds to all emissions <200 kg/hr (i.e. effectively those emissions below the
328 point source detection limit of MethaneAIR that flew in multiple campaigns in the US at 40,000ft above ground
329 level (Chulakadabba et al., 2023)). MethaneAIR characterizes the total regional emissions including the spatial area

emissions at high resolution using a geostatistical inverse modeling framework (Miller et al., 2013) while ingesting high-emitting point source information in the inversion (Chulakadabba et al., 2023; Omara et al., 2024). For Cusworth et al. (2022), we analyze all campaigns by subtracting both aerially detected pipeline emissions and all non-oil/gas emissions (e.g., wastewater, landfills, agriculture), since our study is focused solely on upstream and midstream oil/gas sources. In addition, we subtract emissions from pipelines and non-oil/gas sources emitting below aerial detection limits (i.e., TROPOMI inversions subtracted by aerially detected emissions) by estimating the relative fractions of pipeline and non-oil/gas sources from the aerial detections, with the assumption that these fractions are representative (Table S4). However, this process can introduce additional uncertainties in our comparisons, especially for campaigns where 50% or more of aerially detected emissions were from pipelines or non-oil/gas sources.

We account for the intermittency of detected methane sources with <3 overpasses in Cusworth et al. (2022) by resampling with replacement (n=1,000) the source persistence of methane sources with >3 overpasses for the same campaign, which is consistent with their methodology. We calculate the percentage contributions of low emitting sources in Cusworth et al. (2022) using Eq. (2): where $\%E_{<x}$ is the percentage of total oil/gas methane emissions below an emission rate threshold x (kg/hr), T is the total area emissions measured via TROPOMI inversions (kg/hr), and $P_{>x}$ is the sum of point source emissions above the emission rate threshold x (kg/hr).

$$\%E_{<x} = 1 - \frac{P_{>x}}{T} \quad (2)$$

2.5 Uncertainty calculations

Our emission distributions based on facility-level estimates incorporate uncertainty through several steps, such as the: probabilistic distributions of a select facility being a top 5%, bottom 95% emitter, or facility emitting below the LOD; emission rate and loss rate distributions produced from facility-level empirical measurements; and flaring combustion efficiencies. In addition, we incorporate uncertainties from the empirical measurements into our facility-level model by simulating new empirical emission rates based on the associated method uncertainties. At the beginning of each of the 500 model iterations, we use the reported empirical methane emission rate data and estimate a new emission rate using a normal distribution with the mean as the initial reported emission rate and the standard deviation as a percentage of the mean value. These measurement uncertainties (i.e., 1-sigma) are chosen based on the measurement methodology using the lower percentage uncertainty ranges provided by Fox et al. (2019) for facilities measured via the OTM-33a ($\pm 25\%$), Gaussian plume dispersion ($\pm 50\%$), and tracer release ($\pm 20\%$) methods. For HiFlow sampler measurements, we use an uncertainty range of $\pm 16\%$ (Riddick et al., 2022), and for chamber-based measurements, we use $\pm 14\%$ (Williams et al., 2023). (Riddick et al., 2022), and for chamber-based measurements, we use $\pm 14\%$ (Williams et al., 2023). Therefore, each model iteration incorporates a unique suite of empirical measurement data based on the initially reported emissions and their associated uncertainties, which in turn impacts the probabilistic modeling of the chance of a facility emitting below the method LOD, the empirical

365 data is used to determine the parameters of the lognormal distributions of loss rates and emission rates, and the
366 ranges of the production bins (SI—Section 1). To calculate the cumulative uncertainty of our facility-level model
367 estimates, we estimate 500 methane emission distributions and aggregate the 2.5th and 97.5th percentiles of our
368 ~~five~~even primary facility categories (i.e., low and non-low producing well sites, G&B compressors, T&S
369 compressors, and processing plants), ~~including which include lit and unlit~~ VIIRS flare detection emissions, to
370 determine our 95% confidence intervals. This process is repeated for all simulations at the national-, basin-, and
371 aerial remote sensing boundary levels. For uncertainty calculations in satellite- and aerial-remote sensing studies we
372 use for comparisons, we present the reported 95% confidence intervals, if available.

373 ~~We calculate the 95% confidence intervals for data from MethaneAIR and Cusworth et al. (2022) using the ratio~~
374 ~~of measured point sources to the upper and lower uncertainty bounds of the total area estimates in the calculations of~~
375 ~~the percentage contributions of low-emitting methane sources to the total. In cases where multiple aerial campaigns~~
376 ~~were conducted in the same oil/gas basin by the same study, we average the percentage contributions for all surveys~~
377 ~~including the upper and lower uncertainty bounds. For Cusworth et al. (2022), we do not use the reported~~
378 ~~uncertainty intervals of their point source detections in our uncertainty calculations since we employ various~~
379 ~~emission rate thresholds in our comparisons without a clear understanding of how the point source uncertainties~~
380 ~~would change depending on the different thresholds, meaning that our uncertainty bounds for the Cusworth et al.~~
381 ~~(2022) results may be conservative.~~

382

383 3 Results

384

385 3.1 Distribution of emission rates at the national scale

386

387

388 Based on the results from our facility-level model estimates, we estimate that 70% (95% confidence
389 interval: 61-81%) of total methane emissions from the upstream/midstream sector in the CONUS for 2021 originate
390 from facilities emitting methane at rates <100 kg/hr (Fig. 3). For other emission rate thresholds, we find that 30%
391 (26-34%) of total emissions come from facilities emitting <10 kg/hr, which corresponds to the lower thresholds of
392 aircraft-based aerial remote sensing studies (Cusworth et al., 2022; Johnson et al., 2021; Kunkel et al., 2023; Thorpe
393 et al., 2024; Xia et al., 2024), and 79% (68-90%) of total emissions come from facilities emitting <200 kg/hr. We
394 find that the emission rate threshold corresponding to 50% of cumulative methane emissions from
395 upstream/midstream facilities in the CONUS for year 2021 is 25 kg/hr (19-33 kg/hr). These results suggest that a
396 large majority of oil/gas emissions in the CONUS are not detectable by existing satellite remote-sensing point

Formatted: Font: Times, 12 pt, Not Bold, Font color: Auto

Formatted: Normal

source imagers (Sherwin et al., 2023).

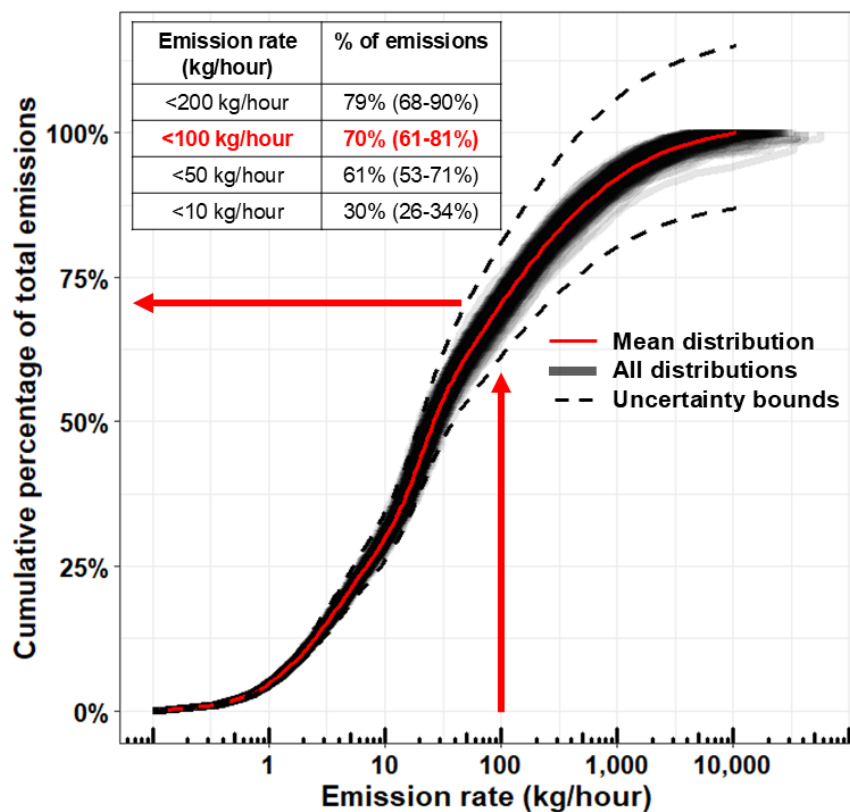
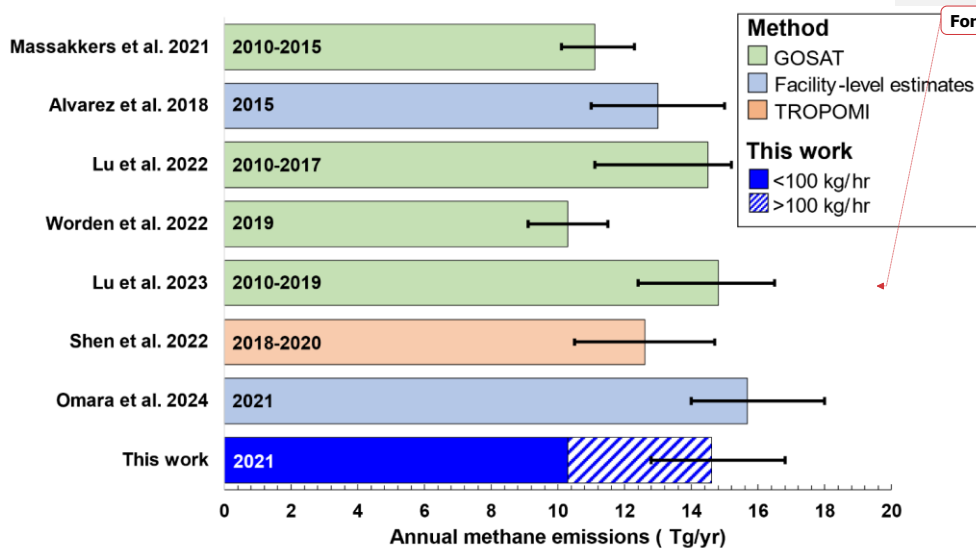


Figure 3: Results from 500 estimated facility-level emission distributions showing the cumulative percentages of total methane emissions contributed from facilities emitting below methane emission rate thresholds. For example, facilities emitting <100 kg/hr account for 72% (63-82%) (61-81%) of total methane emissions. The inset table in the upper left displays the total percentage of methane emissions contributed from several discrete emission rate thresholds with 95% confidence intervals shown in parenthesis.

The distribution for our national-level methane emissions follows an S-shaped curve, noting that the x-axis (i.e., facility-level methane emission rates) is presented in the \log_{10} scale. From 0.1 to 1 kg/hr, we observe a plateau in the distribution curve indicating that increasing emission rates within this range do not significantly increase the percentage contribution to total regional emissions (Fig. 3), similar to the findings in Ravikumar et al. (2019). From 1 to 100 kg/hr, we see a sharper rise in the emission distribution, indicating that increasing emission rates at this range lead to a more substantial contribution to total methane emissions, and account for 68% (60 – 75%) of total methane

411 emissions (Fig. 3, Table S4). Above an emission rate threshold of 100 kg/hr, we see an exponential decline in the
412 percentage contributions of total emission with increasing emission rates, with total methane emissions in this range
413 amounting to 28% (18 – 37%) of the total oil/gas emissions. Facilities emitting at the 1-10 kg/hr and 100-1,000 kg/hr
414 ranges contribute a similar cumulative percentage at 26% (23 - 29%) and 22% (18 - 26%) respectively. Similar
415 percentage contributions are also observed between the 0.1-1 kg/hr and >1,000 kg/hr ranges at 4.5% (4.0 - 5.1%) and
416 6.1% (2.6 - 13%) respectively. Overall, we find that the highest contribution to total national CONUS methane
417 emissions occurs from facilities emitting in the 10-100 kg/hr range at 42% (37 - 46%). In terms of facility counts,
418 from the 673,940 total active oil/gas facilities we estimate in the CONUS for 2021, we estimate that essentially all
419 (i.e., ~99.9%) of these facilities emit methane below 100 kg/hr.

420 Our facility-level model estimates total methane emissions from US upstream/midstream oil/gas emissions
421 for 2021 to be 14.6 (12.7 - 16.8) Tg/yr, or 1,668,000 (1,453,000 – 1,921,000) kg/hr (Fig. 4), which corresponds to a
422 gross gas production normalized loss rate of 2.4%, assuming a uniform 80% methane content in natural gas across
423 oil/gas producing regions in the CONUS. This national emission total of 14.6 (12.7 - 16.8) Tg/yr is more than
424 double the EPA Greenhouse Gas Inventory Report for natural gas and petroleum systems in 2021, excluding post-
425 meter and distribution methane emissions (Inventory of U.S. Greenhouse Gas Emissions and Sinks, 2024). We
426 compare our total national estimates to previous estimates by seven studies that predominantly utilize satellite-based
427 remote-sensing platforms such as GOSAT and TROPOMI inversions (Lu et al., 2022, 2023; Maasakkers et al.,
428 2021; Shen et al., 2022; Worden et al., 2022) except for Alvarez et al. (2018) and Omara et al. (2024) who developed
429 unique facility-based modeling approaches using empirical measurement data collected from multiple oil/gas basins
430 in the CONUS (Fig. 4). Our estimate of national methane emissions overlaps with six out of seven other national
431 estimates of oil/gas methane emissions for the US, with a combined average of 13.1 (ranging from 11.1 - 15.7)
432 Tg/yr. We do not estimate methane emissions from gathering/transmission/distribution pipelines, post-meter
433 emissions, abandoned oil and gas wells, and refineries due to the scarcity of measurement-based data for these
434 sources. Total methane emissions from these sources emit ~2 Tg/year of methane emissions based on other studies
435 (Williams et al., 2021; Alvarez et al., 2018; Omara et al., 2024; Weller et al., 2020; Inventory of U.S. Greenhouse
436 Gas Emissions and Sinks, 2024). Overall, our total national estimate of CONUS methane emissions for 2021 shows
437 good agreement with multiple independent and recent measurement-based estimates.



438

439 **Figure 4:** Comparison of total CONUS oil/gas emissions for 2021 from this facility-level measurement-based
 440 inventory compared to empirical estimates from other studies. Bars are colored according to the methodology used
 441 to derive the total national estimates, and the years within the bars represent the corresponding time periods for the
 442 estimates. **Black inset lines represent 95% confidence intervals.** Our total estimates for “This work” do not include
 443 emissions from other oil/gas methane sources such as abandoned oil and gas wells,
 444 transmission/gathering/distribution pipelines, post-meter emissions, and refineries. Emission estimates from Omara
 445 et al. (2024) do not include methane emissions from abandoned oil and gas wells. We assume that the remote
 446 sensing estimates (i.e., GOSAT and TROPOMI) include all oil/gas methane sources, including downstream
 447 emissions.

448

449 3.2 Distribution of emission rates at the basin-level scale

450

451 Among the top ~~twelve~~^{nine} emitting oil/gas basins in the CONUS, we observe variations among the
 452 different basins in terms of the methane emission distributions, especially at higher emission rate thresholds (Fig. 5).
 453 The majority of the top ~~twelve~~^{nine} emitting oil/gas basins in Fig. 5 show higher percentage contributions from
 454 facilities emitting <100 kg/hr when compared to our national estimate of ~~72%~~^{63–82}~~70%~~^{61–81} (Fig. 3).
 455 These percentage contributions vary from ~80% in the Permian, Appalachian, and Eagle Ford basins, up to ~90% in
 456 the oil-dominant San Joaquin basin. Only the Anadarko and ~~Denver~~^{Bakken} basins have notably lower contributions
 457 to total emissions at the 100 kg/hr threshold at ~~~65~~^{~60}~~60%~~ compared to the national level, which is still a significant
 458 majority of total methane emissions. Despite these variations, our facility-level model estimates that the majority of
 459 total national oil/gas emissions are consistently contributed from facilities emitting <100 kg/hr for the top ~~twelve~~^{nine}
 460 emitting basins.

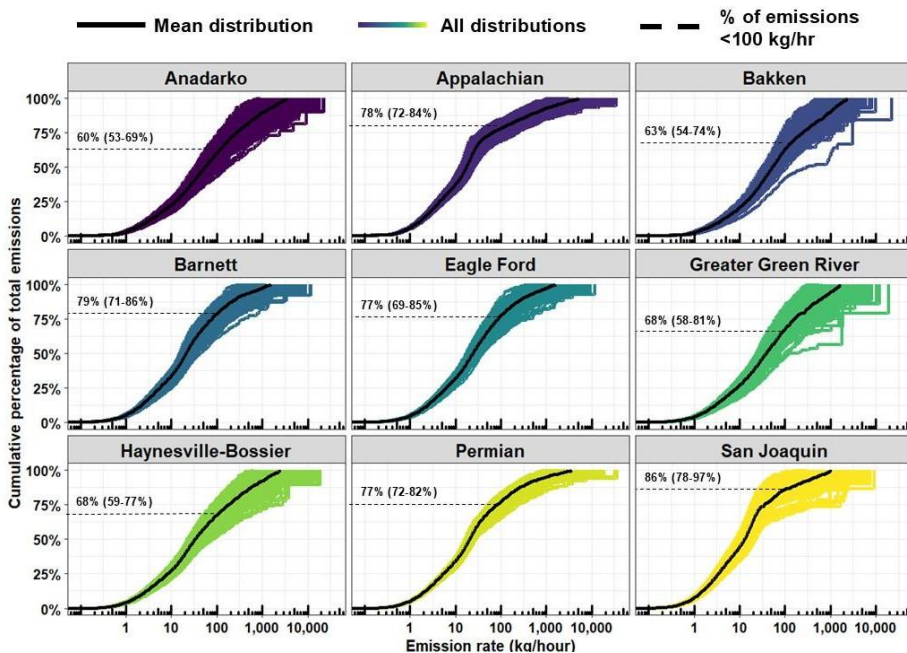
461 Our ~~modeled~~estimated facility-level emission distributions for the top ~~12~~nine emitting oil/gas basins all
462 follow an S-shaped curve (Fig. 5) like the national distribution (Fig. 3), albeit with certain variations. For all basins,
463 the initial plateau in the emissions distribution curves ends at around 1 kg/hr before beginning to rise more steeply.
464 For the Appalachian and San Joaquin basins, the second plateau is at the 20-50 kg/hr emission rate threshold (Fig.
465 5). For the remaining basins, the rise in the emission distribution curves plateaus gradually, indicating a more
466 consistent relationship of emission rate thresholds to their contribution to total emissions. The variability displayed
467 among the 500 basin-level simulations differs among the oil/gas basins, with less spread in the 500 estimated
468 methane emissions distributions for the Appalachian, Anadarko, and Permian basins compared to the Uinta, Denver-
469 Julesburg, and San Joaquin basins (Fig. 5 and Fig. S6). These variations are likely caused in part by the overall total
470 basin-level methane emissions, where an extremely high estimated methane emission rate would have a greater
471 impact on the percentage contribution to the total for basins with lower overall emissions (e.g., the apparent ~~outlier~~
472 ~~distributions present in outliers for the San Joaquin basin~~Greater Green River and Bakken basins in Fig. 5). We
473 discuss below other plausible causes for basin-to-basin variability in the estimated methane emission distributions.

474 In terms of total methane emissions, the top two emitting oil/gas basins are the Permian and Appalachian,
475 which collectively account for ~~5.2~~ (4.4 – 6.3) Tg/year (Fig. S1) or ~~37%~~ of total upstream and midstream oil/gas
476 ~~methane emissions~~. This exceeds the cumulative contribution from the other seven highest emitting oil/gas basins
477 which collectively account for ~~3.7~~ (2.9 – 5.0) Tg/yr. Notably, we find that the highest emissions in the CONUS
478 occur from regions outside of any basin boundary ~~4.3~~ (1.2 – 6.3) Tg/year. Our estimates for basin-level total
479 emissions also show good agreement with remote-sensing satellite-based observations (Fig. S1), except for the
480 Appalachian, Bakken, Greater Green River, and Denver-Julesburg basins where our results are consistently more
481 than double those from the remote-sensing studies that used a prior-emission based inversion result (Lu et al., 2023;
482 Shen et al., 2022). These four basins are in regions with relatively low TROPOMI observation counts and densities
483 compared to other regions in the CONUS (Shen et al., 2022), in addition to other factors that could influence
484 satellite-based inversions such as the presence of many non-oil/gas sources such as coal, livestock, and landfills.
485 Overall, our estimates of total basin-level emissions are consistent with satellite-based observations.

486

487

488



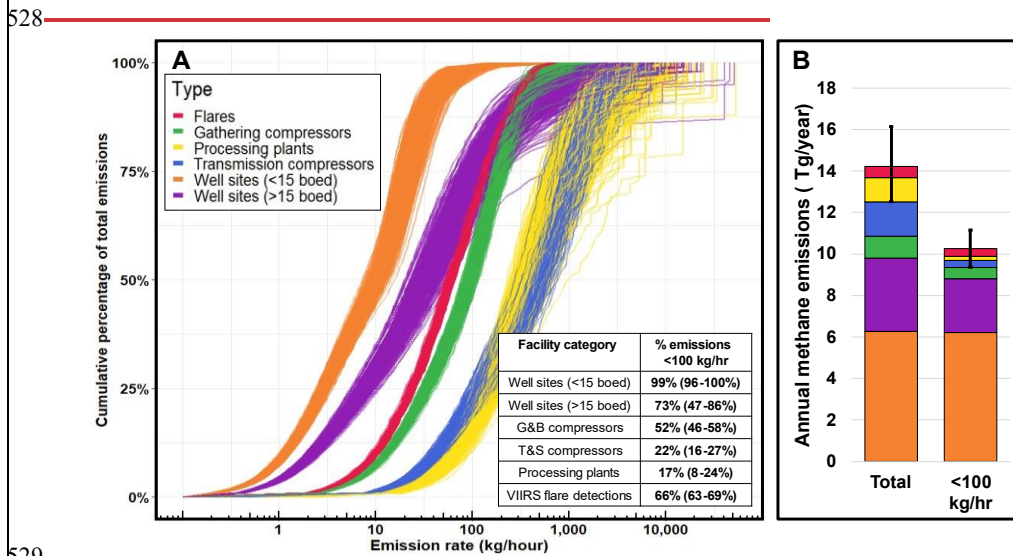
489 **Figure 5:** A) Results from 500 model simulations showing the cumulative methane emissions distribution curves for
 490 total upstream/midstream oil/gas methane emissions for the top nine emitting oil/gas basins in the CONUS for 2021.
 491 The model averages for each basin are shown in solid black lines. Inset dashed lines represent the percentage
 492 contributions of total emission from sources emitting <100 kg/hr. Emission distribution curves for the remaining
 493 eleven oil/gas basins in the CONUS are shown in Fig. S4S6, and a map of the spatial boundaries used for the
 494 different oil/gas basins is shown in Fig. S4S10.

496
 497 **3.3 Distribution of emission rates by facility category**
 498

499 We find significant variations in the methane emission rate distribution curves among the different facility
 500 categories (Fig. 6A). Over 50% of total methane emissions from low (*i.e.* <15 boe/day, or <0.13 kt of methane
 501 production per year and non-low production well sites, lit flares, and G&B compressor stations occur from facilities
 502 emitting <100 kg/hr (Fig. 6A). In contrast, only 17% (8-24|5-18%) of emissions from processing plants and 22%
 503 (16-27, 19% (18-20%)) of emissions from T&S compressor stations, and 9% (7-12%) of emissions from unlit flares
 504 are contributed from facilities emitting <100 kg/hr. Similar variability is also observed at other
 505 emission rate thresholds, such as only 1% (0-2%) of total emissions for T&S compressor stations, unlit flares, and
 506 processing plants originating from facilities emitting at rates <10 kg/hr, compared to 50% (43-58%) from low
 507 producing well sites and 30% (24-35%) from non-low producing well sites (Fig. 6A). At higher emission rate
 508 thresholds, we find that 33% (20-45%) of total emissions from T&S compressors and processing plants are emitted

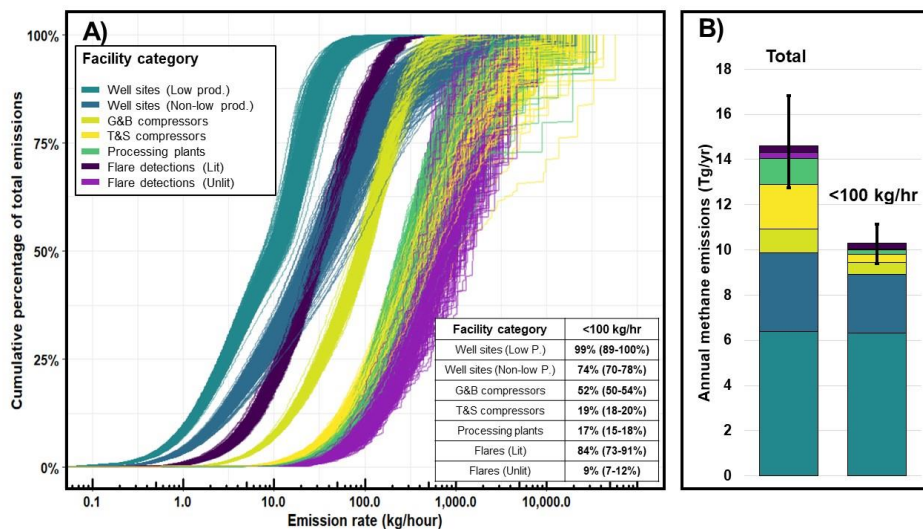
509 from facilities <200 kg/hr, compared to 84% (68-93%) from non-low producing well sites (>15 boedboe/day of
 510 combined oil and gas), 86% (83-88%) from VIIRS flare detections, 78% (70-86%) from G&B compressor stations,
 511 and essentially 100% of emissions from low producing well sites.

512 A breakdown of the 673,940 total facilities in our model has 541,970 as low-producing well sites, followed
 513 by 121,824 non-low-production well sites, 4,181,431 G&B compressor stations 2,033,093 T&S compressor stations,
 514 919 processing plants, and 3,153 total VIIRS flare detections. Of these 673,940 total facilities, 99.5% (99.4 – 99.6%)
 515 emit methane at rates <100 kg/hr (Fig. S11), and in turn contribute 70% of total methane emissions (Fig. 3). Overall,
 516 we estimate that roughly 7068% of total CONUS oil/gas methane emissions for 2021 come from production well
 517 sites, of which 44% are from low-production well sites with combined oil/gas production <15 boedboe/day (i.e.,
 518 <0.13 kt of methane production per year), and the remaining 2624% from non-low production well sites (i.e., >15
 519 boedboe/day) (Fig. 6B). 26Midstream facilities contribute 29% of total methane emissions are from midstream
 520 facilities, with 113% from T&S compressors, 8% from processing plants, 7% from G&B compressor stations, and
 521 the. The remaining 4% from VIIRS flare detections are evenly split with 2% each from lit and unlit flares
 522 respectively. Based on the population counts for each facility category and their corresponding total methane
 523 emissions, the average methane emission rate per facility category is highest for processing plants at 145 (109 –
 524 277)146 (115 – 283) kg/hr, followed by 92 (72 – 118)106 (89 – 129) kg/hr for T&S compressor stations, 28 (26 –
 525 32)27 (25 – 29) kg/hr for G&B compressor stations, 3.3 (2.9 – 3.8)4.9) kg/hr for non-low producing well sites, and
 526 1.3 (1.42 – 1.5) kg/hr for low producing well sites. For VIIRS flares detections, we find a large difference in average
 527 emissions between lit flares at 11 (9.2 – 13) kg/hr and unlit flares at 205 (132 – 294) kg/hr.



529

530 Production well sites constitute the bulk of total methane emissions among the facility categories we
 531 considered, with most of these emissions contributed from low production well sites. Overall, we find that 77% (72-
 532 81%) of well site emissions originated from only 10% of national oil and gas production in 2021 (Fig. S7).
 533 highlighting a disproportionately large fraction of emissions relative to production. In terms of individual well site
 534 level production values, the same 77% (72-81%) of total cumulative methane emissions were contributed from well
 535 sites producing >50 boe/day (i.e., 0.43 kt of methane production per year) or lower. For well sites producing 15
 536 boe/day (i.e., 0.13 kt of methane production per year) or lower, which is the production threshold used to define a
 537 well site as being marginally producing in previous work (Deighton et al., 2020; Omara et al., 2022), we find that
 538 these low producing well sites accounted for 65% (58-69%) of total well site emissions, or 6.4 Tg/yr (4.7-6.8 Tg/yr).



541
 542 **Figure 6:** A) Results from an ensemble of 500 estimated methane emission distributions showing the percentage of
 543 total methane emissions among facility categories contributed from facilities emitting at rates below an emission rate
 544 threshold. The inset table on the bottom right displays the discrete percentage contributions to total methane
 545 emissions contributed from facilities emitting <100 kg/hr. B) Breakdown of total annual methane emissions
 546 contributed from all emitting facility categories and those emitting at rates <100 kg/hr.

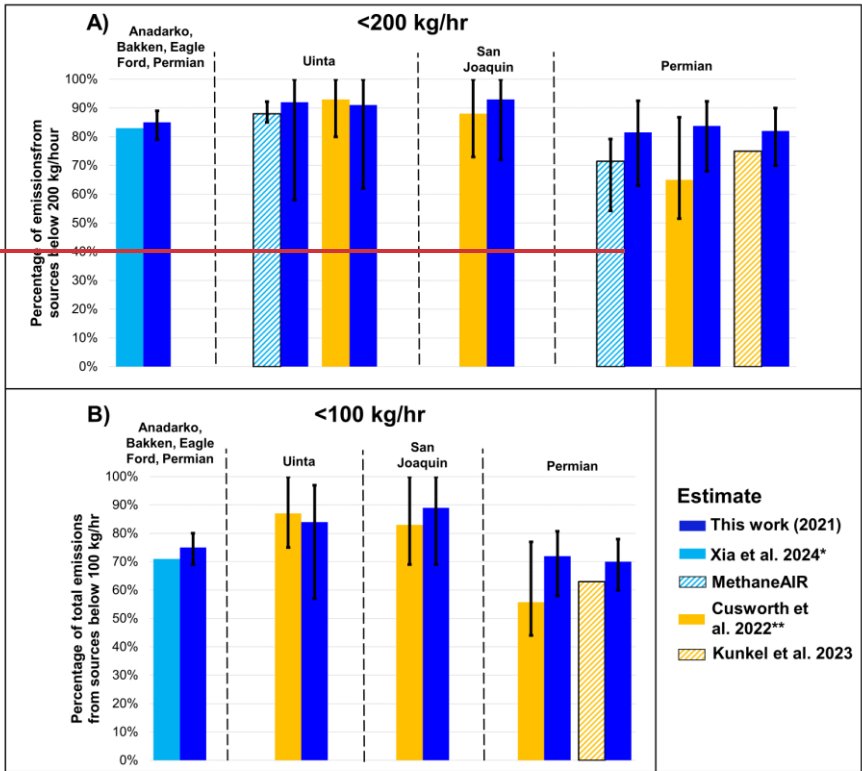
547 **Only single percentiles are used for the y-axis in A) due to the large volume of data (i.e., ~2 million data points) available for the figure. The use*
 548 *of single percentiles causes instances of duplicated emission rates for ascending percentiles at upper emission rate thresholds for different facility*
 549 *categories, leading to the appearance of segmented methane emissions distribution curves for some facility categories.*

550 ***Note that the emission distributions for flares represent VIIRS flare detections which could include multiple*

552 In a comparison of the percentage contributions to total emissions from low-emitting sources between our
553 facility-level model estimates and the aerial remote sensing campaigns presented in Fig. 7, we find that point source
554 contributions are comparable across the aerial remote sensing campaigns. Our comparisons to the available flight
555 results from MethaneAIR, which quantifies both total regional methane emissions and high-emitting point sources
556 >200 kg/hr from the same aerial platform (Chulakadabba et al., 2023), show close agreement between our facility-
557 level estimates and the only available MethaneAIR campaigns in the Uinta and Permian basins for facilities emitting
558 <200 kg/hr (Fig. 7A). For the MethaneAIR flight in the Uinta basin, we estimate that 92% (58–100%) of total
559 oil/gas methane emissions are from sources emitting <200 kg/hr compared to 88% (85–92%) from MethaneAIR
560 (Fig. 7A). For the two available flights in the Permian basin from MethaneAIR, we estimate total contributions from
561 <200 kg/hr sources at 82% (63–93%) compared to the 72% estimated by MethaneAIR (Fig. 7A).

562 We see close agreement between our facility-level methane emission distribution curves and the observed
563 emissions by Bridger GML in the four-basin aggregate provided by Xia et al. (2024) (Fig. S14A) and the Permian
564 remote sampling campaign (Fig. S14B) by Kunkel et al. (2023), with the measured emissions from the Bridger
565 GML surveys overlapping with our facility-level model simulations throughout the continuous distribution of
566 methane emission rates.

569



570

571

572 3.4 Comparisons to aerial remote sensing studies

573

574 We perform comparisons of the percentage contributions of methane emissions from facilities emitting
575 below discrete emission rate thresholds between seven aerial remote sensing campaigns across four distinct regions
576 and our estimated facility-level results (Fig. 7). The aerial remote sensing technologies include data from Bridger
577 GML measurements (Kunkel et al., 2023; Xia et al., 2024), MethaneAIR (Omara et al. 2024; Miller et al. 2023), and
578 the results from Global Airborne Observatory and next-generation Airborne Visible/Infrared Imaging Spectrometer
579 campaigns (Cusworth et al., 2022) which are also included in the aerial detections used by Sherwin et al. (2024). [In](#)
580 [comparing the percentage contributions to total emissions from low-emitting sources between our facility-level](#)
581 [estimates and the aerial remote sensing campaigns, we find that emission contributions agree well across aerial](#)

582 [remote sensing campaigns for the total percentage of methane emissions from facilities emitting, as seen in Fig. 7](#)
583 [for both less than 100 kg/hr and 200 kg/hr.](#)

584 For the Bridger GML remote sensing campaigns (Kunkel et al., 2023; Xia et al., 2024), we find good
585 agreement in the percentage of total emissions contributed from facilities emitting <200 and <100 kg/hr compared to
586 our facility-level model estimates (Fig. 7). A comparison of continuous emissions distribution curves between our
587 facility-level emission distributions and two Bridger GML aerial remote sensing campaigns (Kunkel et al., 2023;
588 Xia et al., 2024) targeting four oil/gas basins is shown in Fig. S3. The Bridger GML aerial sampling platform has the
589 lowest LOD among the aerial campaigns we analyze in this work and a similar source resolution (i.e., 30 meters) to
590 our facility-level model (i.e., 50 meters), allowing for a more detailed comparison of continuous emission
591 distribution curves due to the higher number of detected methane sources at low emission rates provided by Bridger
592 GML surveys. [We find close agreement between our facility-level methane emission distribution curves and the](#)
593 [observed emissions by Bridger GML in the four-basin aggregate provided by Xia et al. \(2024\) \(Fig. S3A\) which](#)
594 [includes Anadarko, Bakken, Eagle Ford and Permian basins \(individual basin data are not currently available in Xia](#)
595 [et al. \(2024\)\), as well as separately for the Permian remote sampling campaign \(Fig. S3B\) by Kunkel et al. \(2023\),](#)
596 [with the measured emissions from the Bridger GML surveys overlapping with our facility-level model simulations](#)
597 [throughout the continuous distribution of methane emission rates.](#)

598 For the multiple aerial remote sensing campaigns performed by Cusworth et al. (2022), we generally find
599 good agreement with all of our estimates statistically overlapping for discrete emissions rate thresholds of <100
600 kg/hr and <200 kg/hr [for the Permian and Uinta oil/gas basins \(Fig. 7\). For the San Joaquin and Denver-Julesburg](#)
601 [oil/gas basins, we see good agreement at the emission rate threshold of <200 kg/hr and at <100 kg/hr \(i.e.](#)
602 [overlapping uncertainty bounds\). For the Appalachian basin, we find broad agreement at both emission rate](#)
603 [thresholds of <100 kg/hr and <200 kg/hr, with our results consistently showing a 20-30% greater contribution from](#)
604 [emission sources below the discrete emission rate thresholds \(Fig. 7\). We find the closest agreement in the Permian](#)
605 [and Uinta oil/basins, where the differences in the average percentage contributions vary from -9% to +4% across the](#)
606 [three discrete emission rate thresholds of <100 and <200 kg/hr \(Fig. 7\). In Denver-Julesburg and Appalachian](#)
607 [basins, the differences are observed to be larger, compared to other basins, where the differences in average](#)
608 [percentage contributions across the discrete emission thresholds vary from -30% to +18%, however, they are within](#)
609 [our estimated uncertainty bounds. The detected point sources by Cusworth et al. \(2022\) in the Denver-Julesburg and](#)
610 [Appalachian basins contain many non-oil/gas point sources \(Table S4\), which may lead to additional uncertainty in](#)
611 [the comparisons for these basins since we use the relative proportions of point sources to subtract an estimated](#)
612 [contribution of non-oil/gas point sources from the TROPOMI estimates to provide a more direct comparison](#)
613 [between our estimates \(since our study only focuses on upstream and midstream oil and gas sectors\) and those of](#)
614 [Cusworth et al. \(2022\). Notably, the Appalachian basin contains the highest percentage contribution of non-oil/gas](#)
615 [point sources at 67% \(Table S4\). In contrast, we note that all of the detected point sources by Cusworth et al. \(2022\)](#)
616 [in the Permian and Uinta basins were attributed to oil/gas point sources \(Table S4\).](#)

Our comparisons to the available flight results from MethaneAIR, which quantifies both total regional methane emissions and high-emitting point sources >200 kg/hr from the same aerial platform (Chulakadabba et al., 2023), show close agreement between our facility-level estimates and the available aerial campaigns in the Uinta and Permian basins for facilities emitting <200 kg/hr (Fig. 7B). For the MethaneAIR flight in the Uinta basin, we estimate that 92% (46 - 100%) of total oil/gas methane emissions are from sources emitting <200 kg/hr, compared to 88% from MethaneAIR (Fig. 7B). For the available flight in the Permian basin from MethaneAIR, we estimate total contributions from sources emitting <200 kg/hr at 77% (59 - 90%) compared to the 71% estimated by MethaneAIR (Fig. 7B).

Overall, our findings show that our facility-level estimates closely agree with the results from multiple aerial remote sensing campaigns from different regions and using various measurement methods.

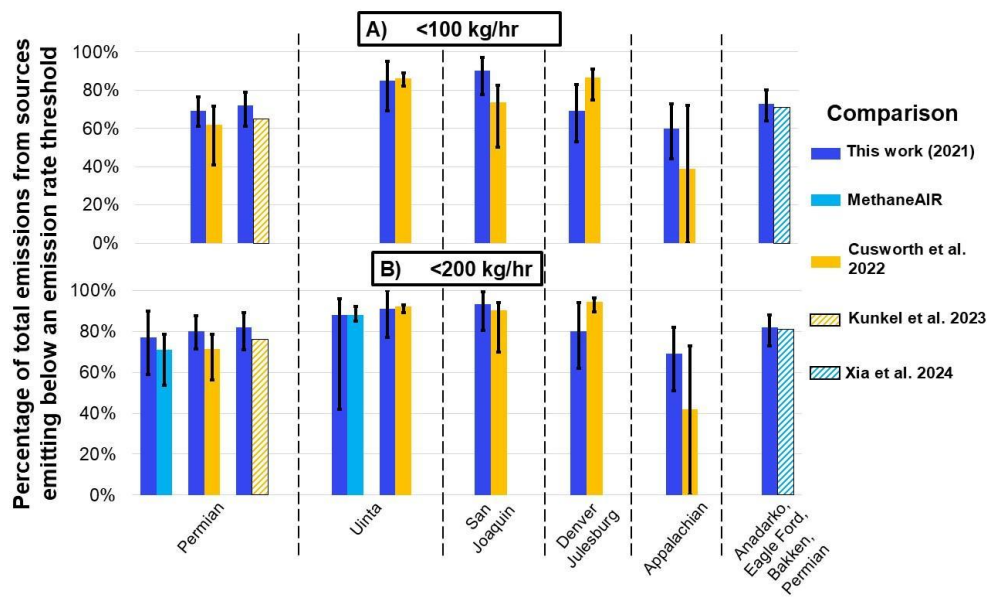


Figure 7: Comparisons of the cumulative percentage of oil/gas methane emissions from all oil/gas facilities emitting <200 kg/hr (A) and <100 kg/hr (B) between our facility-level empirical emissions estimates and aerial remote sensing campaigns. Bars are colored according to the study and grouped according to the target oil/gas basin(s). All results from the facility-level simulations (i.e., this work) are constrained to the spatial boundaries of the aerial campaigns for direct comparisons (note that for a given basin, spatial boundaries might be slightly different). Uncertainty bars for the facility-level simulations are the 2.5th and 97.5th percentiles of 500 simulations. Maps of all spatial boundaries used for comparisons are provided in Fig. S2. Comparisons to MethaneAIR are not

636 performed at the <100 kg/hr threshold because MethaneAIR detections are not available for point sources below
637 this emission rate threshold.

638 *The surveyed oil/gas basins in Xia et al. (2024) are the Anadarko, Bakken, Eagle Ford, and Permian basins. The exact surveyed boundaries are
639 not available from Xia et al. (2024); therefore the comparisons between this work are for the entire four oil/gas basins.

640 **Results presented by Cusworth et al. (2022) in the Permian oil/gas basin are the average of four Permian aerial remote sensing campaigns.

642 4 Discussion

644 Understanding how facilities with different magnitudes of emissions contribute to total regional emissions
645 has direct policy implications for methane quantification and mitigation, such as the selection of
646 measurement/screening methods with the appropriate detection sensitivities (Ravikumar et al., 2018). We find that
647 roughly three-quarters of total oil/gas methane emissions from the upstream/midstream sectors come from facilities
648 emitting at rates <100 kg/hr. Facility-level, measurement-based data collected in some other countries present a
649 similar story. Our main finding is that 70% of total oil/gas methane emissions from the upstream/midstream sectors
650 come from facilities emitting at rates <100 kg/hr, which is the emission rate threshold above which point source
651 emissions are referred to as “super-emitting” oil/gas source by the EPA (Standards of Performance for New,
652 Reconstructed, and Modified Sources and Emissions Guidelines for Existing Sources: Oil and Natural Gas Sector
653 Climate Review, 2024). While detecting and mitigating emissions from super emitters are important (Cusworth et
654 al., 2022; Duren et al., 2019; Sherwin et al., 2024), our results underscore the need to account for oil/gas methane
655 sources emitting at lower rates, as the cumulative contribution of lower-emitting sites accounts for a large majority
656 of emissions across US oil/gas basins. Facility-level, measurement-based data collected in other countries present a
657 similar story. From a sample of sites (n=302) measured via Bridger GML remote sensing platform in British
658 Columbia, Canada (Tyner and Johnson, 2021), roughly 60% of the total quantified oil/gas site-level emissions
659 originate from sites emitting <32 kg/hr. In Romania, a site-level measurement-based inventory (Stavropoulou et al.,
660 2023) using 178 measurements finds that oil production facilities emitting <100 kg/hr contribute 78% of total oil/gas
661 methane emissions in the studied region. In short, the high percentage contribution from lower-emitting (<100
662 kg/hr) oil/gas facilities that account for a large majority of total emissions is not unique to the US and is likely
663 present in other countries as well. A combination of approaches that characterize entire emission distributions across
664 populations of sites (i.e., not just focusing on measuring super-emitters) and quantification of regional-level
665 emissions is needed in other countries to quantify the relative contributions of low-emitting sources that in aggregate
666 can be significant sources of overall oil/gas methane emissions.

667 While most of the focus in this work centers around quantifying the percentage contributions of oil/gas
668 methane sources emitting below one discrete emission rate threshold (i.e., <100 kg/hr, per EPA’s definition of a
669 super-emitter) our assessment illustrates the importance of a complete characterization of emissions which gains
670 importance as newer methane monitoring technologies have different LODs. Most of our analysis centers around
671 quantifying the percentage contributions of oil/gas methane sources emitting below one discrete emission rate

672 [threshold \(i.e., <100 kg/hr, per EPA’s definition of a super-emitter\). We estimate that over 99% of the total oil/gas](#)
673 [facilities that we analyze in this work emit below 100 kg/hr \(Fig. S11\), which in turn contribute 70% \(61 – 81%\) of](#)
674 [total methane emissions \(Fig. 3\). The emission rate threshold of 100 kg/hr is relevant to US policy decisions \(EPA’s](#)
675 [Final Rule for Oil and Natural Gas Operations Will Sharply Reduce Methane and Other Harmful Pollution., 2024\).](#)
676 [but we also illustrate the importance of a complete characterization of emissions, which gains importance as newer](#)
677 [methane monitoring technologies have different LODs.](#) For example, the effective LOD at high probabilities of
678 detection for available point source imaging satellites of ~200 kg/hr (Jacob et al., 2022) would only be able to
679 quantify 21% (10-32%) of all oil/gas point sources in the CONUS, if the full oil/gas sector was mapped in its
680 entirety, based on our facility-level results. [When considering the relationship of facility-level emission rates to total](#)
681 [cumulative methane emissions, we find that oil/gas methane emissions in the CONUS are dominated by many low-](#)
682 [emitting facilities, which relates directly to methane measurement technologies.](#)

683 Point source-focused remote sensing platforms offer the advantage of rapidly surveying large areas (i.e.,
684 100’s-1,000’s km²) which facilitates the detection and quantification of high-emitting point sources (Cusworth et al.,
685 2022; Duren et al., 2019; Sherwin et al., 2024). In contrast, logistical constraints often limit the sample sizes for
686 ground-based vehicle sampling platforms, however, these limitations can be overcome with stratified random,
687 representative sampling and statistical analysis approaches like this work. Ground-based measurement platforms
688 provide much lower LODs (i.e., <1 kg/hr) when compared to remote sensing platforms, which are necessary to
689 quantify emissions from the large number of small methane sources we find that contribute roughly three-quarters of
690 total regional oil/gas emissions in the CONUS and will only improve as additional ground-based measurements are
691 gathered. Overall, our main findings highlight the importance of methods that can rapidly locate the small number of
692 high-emitting point sources we estimate, but our findings emphasize the need to account for the disproportionately
693 large majority percentage of total regional oil/gas emissions that are emitted from smaller diffuse methane sources.

694 _____ When extrapolating our facility-level model results to the basin-level we see variations among the emission
695 distribution curves for different oil/gas basins, but still find that most methane emissions come from facilities
696 emitting <100 kg/hr. The variations in the emission distribution curves for different basins are driven by many
697 factors, such as the: production characteristics, number and density of facilities, different types and relative counts of
698 facility categories, the availability of empirical measurement data used to model emissions, and the total oil/gas
699 methane emissions (i.e., the denominator). For example, the Appalachian basin is dominated by a high number of
700 older low-production well sites (Deighton et al., 2020; Riddick et al., 2019; Enverus, 2024) with fewer midstream
701 facilities such as processing plants and G&B compressors, which contrasts with the Bakken basin where we find a
702 high number of midstream facilities, high-producing well sites, and VIIRS flare detections ([Elvidge et al., 2016;](#)
703 [Enverus, 2024](#)), ([Elvidge et al., 2015; Enverus, 2024](#)). When comparing the emissions distribution curves for the
704 Bakken and Appalachian basins (Fig. 5), we observe higher contributions from lower-emitting facilities for the
705 Appalachian compared to the Bakken. An example of differences in basin-level production is shown in Fig. [S9S4](#)
706 and Fig. [S10S5](#), where we see variable profiles among the different oil and gas-producing basins in terms of well
707 site production characteristics, which are the main source of total methane emissions in this work (Fig. 6). We also

708 observe the influence of total basin-level emissions on the variability among our emission distribution curves, where
709 large emitting sources in the San Joaquin basin can lead to high variability among the estimated emission
710 distribution curves compared to the Permian basin which has roughly ten times the total emissions compared to the
711 San Joaquin (Fig. 5). We note that a direct comparison of our model results with aerial remote sensing methods may
712 be limited, in part, by methodological differences in methane quantification approaches (and underlying
713 uncertainties). The remote sensing observations assessed here as snapshots may capture facility-level emission
714 distributions that are not well represented in annually averaged methane emissions distributions, as we estimate here.
715 Nevertheless, we find broad agreement with these independent aerial remote sensing estimates at the basin scale and
716 across smaller spatial domains, as discussed. Ultimately, as many characteristics will influence methane emissions
717 distribution curves among different oil/gas producing regions in the CONUS, mitigation strategies will need to be
718 structured accordingly to the region they are targeting.

719 Our results find that over half of cumulative methane emissions from three different facility categories
720 come from facilities emitting <100 kg/hr, including methane emissions from [VHRS flare-detections-lit and unlit](#)
721 [flares](#). We show how the large contributions from small methane sources to total regional emissions are not unique
722 to any one facility category, but it is important to contextualize our emission distribution curves with the
723 corresponding total regional emissions. Our facility-level estimates find that the main source of oil/gas methane
724 emissions in the CONUS are oil/gas production well sites, of which the low production category is responsible for
725 44% (39 – 49%) of the total estimated oil/gas methane emissions in the CONUS in 2021. Low-producing well sites,
726 also known as “marginal wells”, have been shown in previous work to be a significant source of methane emissions,
727 especially relative to their contribution to overall oil/gas production ([Omara et al., 2022; Deighton et al., 2020](#)),
728 [Omara et al. \(Deighton et al., 2020; Omara et al., 2022\)](#). [Omara et al. \(2022\)](#) found that marginal wells contributed
729 anywhere from 37%-75% of total methane emissions from production well sites, which is ~~similar to~~like our
730 estimates (i.e., ~~6465~~6%). Despite low production well sites having a lower mean emission rate compared to other
731 facility categories, the large facility counts result in significant aggregate total emissions of methane. This implies
732 that detection and mitigation strategies to reduce methane emissions from these and other low-emitting oil and gas
733 infrastructure (e.g., abandoned oil/gas wells) would require alternative mitigation and detection approaches
734 compared to those for the small number of super-emitting emission sources. For detection, measurement methods
735 that can measure emission rates between 0.1-100 kg/hr are required, since this range makes up ~~7270~~70% of total
736 methane emissions ([Fig-Figure 3 and Table S1](#)) as modeled herein. In terms of methane mitigation policy, financial
737 incentives, like the USD 4.7 billion from the Biden Bipartisan Infrastructure Law for abandoned wells, could be
738 used to prioritize the repair of old and leak-prone production well sites, as these low-producing well sites only
739 account for a small fraction (i.e., ~~5.6% in 2019~~5.6% in 2019) of total oil/gas production ([Omara et al., 2022](#)), ~~5.6% in 2019~~ of
740 total oil/gas production ([Omara et al., 2022](#)).

741 We see good agreement between our facility-level-model results and a majority of aerial remote sensing studies,
742 which are expected to capture a wide range of high-emitting facilities in a survey region. For example, when
743 comparing our model results to Kunkel et al. (2023) and Xia et al. (2024) we find that our estimated methane

744 emissions closely match the distribution of methane emissions measured in Bridger GML surveys (Fig. S14). In the
745 same analysis, we estimate nearly identical total emissions from facilities emitting >100 kg/hr when compared to the
746 results of Kunkel et al. (2023), S3). We also find good agreement to satellite remote sensing estimates of emissions,
747 such as our basin-level (Fig. S1) and national-level comparison to satellite inversions (Fig. 3), and other aerial
748 remote sensing study regions (Table S2). Our comparisons of the contributions of low-emitting sources below
749 discrete emission rate thresholds also agree closely with recent MethaneAIR, Kairos Aerospace, GAO, and AVIRIS-
750 NG aerial surveys, whose results also highlight the importance of small methane sources to overall oil/gas methane
751 emissions. This broad agreement across multiple studies differs from those of Sherwin et al. (2024) who suggest
752 majority of total emissions from a small fraction of high-emitting sites. Notably, many of the same aerial
753 measurements that are used in Sherwin et al. (2024) are used for comparisons in this work (i.e., Cusworth et al.
754 (2022)) (Fig. 7) that appear to indicate that the estimation of the overall methane emissions from small emitting
755 sources in Sherwin et al. (2024), in particular those below aerial detection limits used in their study, may be an
756 underestimate. Recently, Sherwin et al. (2024) suggested that a majority of total emissions originate from a small
757 fraction of high-emitting sites. Notably, most of the aerial measurements that are used in Sherwin et al. (2024) are
758 obtained from the Cusworth et al. (2022) study, with which we see good agreement (Fig. 7). Sherwin et al. (2024)
759 perform an alternative analysis than Cusworth et al. (2022) for aerially measured sources with <3 overpasses and
760 assume that sources with one or two overpasses emit at their observed intermittency of 100%, 50%, or 0% of the
761 time. This difference in analytical approaches produces higher contributions from aerial emissions in Sherwin et al.
762 (2024) by 31% on average for seven aerial campaigns compared to Cusworth et al. (2022) (Table S7), which uses a
763 resampling approach described earlier in the Methods Section 2.4. In addition, emissions from Sherwin et al. (2024)
764 that are below aerial detection limits are estimated using a combination of an equipment-level bottom-up model
765 presented in Rutherford et al. (2021) for production well sites, and emission factors from the U.S. Greenhouse Gas
766 Inventory (Inventory of U.S. Greenhouse Gas Emissions and Sinks, 2024) for midstream facilities, which produces
767 52% lower emissions on average for seven aerial campaigns (Table S7). Therefore, the aerially measured emissions
768 in Sherwin et al. (2024) are higher and the emissions below aerial detection limits are lower which leads to a higher
769 contribution to total methane emissions from high-emitting facilities (Table S7). Ultimately, the broad agreement we
770 find across multiple disparate measurement techniques and platforms across Bridger GML aerial campaigns (Kunkel
771 et al., 2023; Xia et al., 2024), MethaneAIR measurements (MethaneAIR L4 Area Sources 2021 | Earth Engine Data
772 Catalog, 2024; Omara et al., 2024), and the multiple surveyed regions presented in Cusworth et al. (2022), altogether
773 provide collective evidence about the large contribution of smaller emission sources to total regional emissions.

774 The percentage contribution of facilities emitting below an emission rate threshold is a ratio where the numerator
775 is the sum of the total point source emissions (i.e., emissions above an emission rate threshold) and the denominator
776 is the total regional oil/gas emissions. Our comparisons of the percentage contributions of point sources to regional
777 emissions for various aerial remote sensing studies and our facility-level estimates agree. It is worth noting that our
778 calculations of the point source percentage contributions from the aerial remote sensing studies assume that the
779 regional estimate (i.e., the denominator) is entirely from oil/gas sources, which may be reasonable for the Permian
780 basin but is likely not the case for the San Joaquin basin which contains multiple significant non-oil/gas methane

781 ~~sources. These remote sensing studies largely rely on aerial detections of generally higher-emitting point sources as~~
782 ~~part of their numerator, which has~~ Given the variability in methane detection technologies, a range of approaches can
783 be taken to estimate methane emission rate distributions, each providing unique advantages and disadvantages.
784 MethaneAIR provides a novel remote sensing approach where high-emitting point sources, distributed area sources
785 and total regional emissions are quantified using the same aerial platform, providing the ability to directly measure
786 high-emitting point source and diffuse area contributions to total regional estimates. In the work by Xia et al. (2024)
787 they combine measurements from Bridger GML across four oil/gas basins and use component-level simulations to
788 account for facilities emitting below the 3 kg/hr LOD of Bridger GML. Other approaches also exist, such as Cusworth
789 et al. (2022) who combine TROPOMI inversions to estimate total regional methane emissions with point source
790 emissions quantified from their aerial detection platforms (i.e., GAO, AVIRIS-NG). Similarly, Sherwin et al. (2024)
791 combine point source emissions measured via aerial remote sensing with site/facility-level emission rates estimates
792 calculated from a combination of an equipment-level bottom-up model for production well sites (Rutherford et al.,
793 2021) and emission factors from the 2023 GHGI for midstream facilities (Inventory of U.S. Greenhouse Gas Emissions
794 and Sinks, 2024) for facilities emitting below aerial detection limits. Remote sensing studies have key advantages over
795 ground-based sampling platforms, such as rapidly surveying wide areas and capturing higher-emitting point sources,
796 but have variable LODs depending on the target region, topography, measurement technology, presence of co-located
797 non-oil/gas methane sources (i.e., source attribution), weather conditions, infrastructure density, and infrastructure
798 type(s). These variables pose additional challenges when quantifying the contributions from facilities emitting
799 above/below specific emission rate thresholds, which are critical information to inform mitigation policy. Assessing
800 performance, tracking mitigation, and accurate reporting requires building a comprehensive picture of emissions by
801 characterizing all emitters big and small, and reconciling with total basin/sub-basin level emissions. Ultimately, the
802 key seems to be merging the best data from both approaches to build a hybrid inventory, ideally using a multi-tiered
803 system with multiple methods that span a range of LODs that allow for gathering empirical measurements from
804 facilities emitting at all parts of the methane emission distribution curve. Our study is a step in that direction
805 considering measurement-based data while ~~also~~ presenting a robust comparison with available independent remote
806 sensing measurements. At the same time, large-area aggregate emissions data obtained from wide-area remote sensing
807 mapping or mass balance surveys can better constrain total regional emissions (e.g. Cusworth et al. 2022; Omara et
808 al. 2024) towards a more empirically robust denominator in characterizing the relative contributions of small emission
809 and high emission sources to total emissions.

810 We show that our facility-level emission models produce national- and basin-level methane emissions estimates
811 that are in good agreement with other independent measurement-based studies. However, we note the following
812 limitations/biases that could be improved with future data collection efforts. The empirical measurements that we
813 use in our model are representative of the year and time they were measured (i.e., 2010-2020), meaning that they
814 would not reflect any updates in regulatory practices or changes in facility operational and emission management
815 practices. Finally, we include a small number (i.e., 5% of total empirical data used in the model) of measurements
816 gathered using ground-based component/source level sampling methods from two studies (Deighton et al., 2020;
817 Riddick et al., 2019). All measurements from these two studies targeted the lowest production cohort of production

818 well sites and exhibited statistically lower emission rates than those gathered using facility-level ground-based
819 methods (Figure S4). In addition, there are variations in the number of production well site empirical measurements
820 among oil/gas basins (Table S3) although a sensitivity analysis shows that excluding data from individual oil/gas
821 basins does not significantly impact our results (Fig. S9). Furthermore, there are several oil/gas methane emission
822 sources that we do not account for in our estimates, which include: gathering/transmission/distribution pipelines, oil
823 refining and transportation, abandoned oil/gas wells, offshore oil/gas infrastructure, post-meter sources, and oil/gas
824 distribution infrastructure in urban areas. For some sources omitted in this work such as abandoned oil/gas wells,
825 their inclusion would likely lead to a higher contribution from low-emitting facilities, since the highest recorded
826 emission rate from an abandoned oil/gas well is 76 kg/hr (Riddick et al., 2024). For others such as oil refineries,
827 their inclusion would likely lead to a lower contribution from small methane sources given their low facility counts
828 and high per-site emissions (Duren et al., 2019). Despite their omissions, total methane emissions from these sources
829 are currently estimated to account for 5-10% (Alvarez et al., 2018; Riddick et al., 2024; Inventory of U.S.
830 Greenhouse Gas Emissions and Sinks, 2024; Williams et al., 2021) of total oil/gas sectoral emissions. Our estimates
831 also utilize empirically measured emission rates from ground-based sampling platforms which are limited in
832 number, especially in the case of processing plants (n=20) and T&S compressor stations (n=50) (Table S2). The
833 empirical data used in our analysis includes a smaller sample of super-emitting facilities relative to those captured
834 by remote sensing platforms (Duren et al., 2019; Sherwin et al., 2024), but our use of production-normalized loss
835 rates and lognormal distributions to estimate facility-level methane emission rates anticipates and accounts for the
836 possibility of finding low-probability, high-magnitude emissions that occur at rates beyond those that appear in our
837 dataset of empirical observations. For example, our highest empirical emission rate is 1,360 kg/hr for a T&S
838 compressor station, whereas our maximum estimated facility-level emission rate across all 500 facility-level
839 emission distribution curves averages 7,500 kg/hr (3,000 - 21,000 kg/hr). Finally, we include a small number (i.e.,
840 5% of total empirical data used in the model) of measurements for production well-sites gathered using ground-
841 based component/source-level sampling methods from two studies (Deighton et al., 2020; Riddick et al., 2019). All
842 measurements from these two studies targeted the lowest production cohort of production well sites and exhibited
843 statistically lower emission rates than those gathered using facility-level ground-based methods for the same well
844 site production cohort, meaning that any bias introduced by the inclusion of these measurements would lead towards
845 the underestimation of total emissions and/or the percentage contributions from low-emitting sources. Despite these
846 limitations, we have shown that our results are broadly in agreement with satellite- and aerial-based remote sensing
847 studies at national/basin/local scales, and other facility-level estimates.

848 Going forward, several approaches can be used to better understand the percentage contributions from facilities
849 emitting at different leak rate thresholds, and ultimately improve our understanding of oil/gas methane emissions in
850 the CONUS and around the world. A combination of multiple satellite and aerial remote sensing approaches and
851 synthesis of their data by bringing in point source detections at multiple thresholds at the same time characterizing
852 total regional emissions as demonstrated using a compilation of multi-scale measurements seems a viable pathway
853 towards building a more complete picture of the overall methane emissions. Combining aerial and satellite remote
854 sensing measurements with ground-based site/facility-level estimates presents itself as an effective next step, as

855 implemented/suggested by prior studies (Allen, 2014; Alvarez et al., 2018). Aerial or satellite remote sensing
856 platforms focused on point source detection offer the ability to rapidly locate the small number of the highest
857 emitting facilities that contribute a disproportionate fraction of emissions, offering valuable data on specific facility
858 locations that allow for rapid mitigation. However, more direct observational approaches are needed to acquire total
859 emissions data which according to this study is dominated by small-emitting sources that are undetected by high-
860 emitting point source detection systems. Facility-level population-based approaches can account for the lower-
861 emitting facilities that contribute the most total oil/gas methane emissions, which is needed for accurate emission
862 reporting and understanding the contributions of total emissions above/below emission rate thresholds. The ground-
863 based estimates can be further constrained by large-area aggregated emission quantification provided by regional
864 remote sensing or mass balance mapping approaches (Shen et al., 2022; Omara et al., 2024; Jacob et al., 2022)
865 towards producing a more robust overall emission quantification.

866 5 Conclusions

867 In conclusion, our work highlights several key aspects of oil/gas methane emission rate distribution curves
868 in the CONUS for 2021, which include:

- 869 1. A large majority (~~72~~70%) of total national continental oil/gas methane emissions in the US originate from
870 ~~low~~lower-emitting facilities (<100 kg/hr).
- 871 2. Emission rate distributions vary among different oil/gas basins, but among the top nine producing basins
872 we consistently find that most methane emissions (~~63%-90~~60%-86%) originate from oil/gas facilities
873 emitting at rates <100 kg/hr.
- 874 3. ~~We estimate that production~~Production well sites ~~emit~~were found to be responsible for 70% of
875 ~~total~~regional oil/gas methane emissions in the CONUS, with 44% contributed, from ~~low producing well~~
876 ~~which the sites (<15 boed) which is nearly half~~that accounted for only 10% of total national US oil/ and gas
877 ~~methane~~production in 2021, disproportionately accounted for 77% (72-81%) of the total well site
878 emissions..
- 879 4. Our results ~~are~~were consistently found to be in ~~broad~~close agreement with those from independent
880 aerial/satellite remote sensing estimates, both in comparing contributions from discrete emission rate
881 thresholds and continuous emissions distribution curves, which emphasize the importance of ~~small~~
882 ~~diffuse~~the large majority contribution of small-emitting methane sources to total oil/gas methane emissions.

883 Our results highlight, and quantify, the significant contributions of the large number of low-emitting oil/gas
884 facilities to total regional/basin/local oil/gas methane emissions in the CONUS for 2021. In addition to the CONUS,
885 the small oil/gas methane sources are likely a significant component of total regional emissions in other countries as
886 well as recent data suggest from Romania and Canada (Stavropoulou et al., 2023; Tyner and Johnson, 2021) and

888 would need to be further investigated to build a comprehensive assessment of small-emitting methane emissions and
889 their relative contributions to total oil/gas methane emissions globally. This work emphasizes the need for multi-
890 scale approaches to quantify total regional oil/gas methane emissions; and at the same time characterize and account
891 for the large contribution from small emission sources dispersed across a wide area, in addition to incorporating data
892 on high-emitting point sources towards producing overall robust methane emission quantification.

893
894 **Data availability**
895 [All 500 full emission rate distributions at the national level are available to download from Zenodo \(link:](https://doi.org/10.5281/zenodo.13314532)
896 [https://doi.org/10.5281/zenodo.13314532\)](https://doi.org/10.5281/zenodo.13314532). All estimated methane emission rate distributions at the ~~national~~, basin,
897 or small target scale are available upon request. Empirical measurement data used in the estimation of the methane
898 emission distribution curves ~~is~~are available from the references listed in Table ~~S1~~, ~~S2~~.

899
900 **Code availability**
901 R code used to create the methane emission distribution curves and figures is available upon reasonable request.

902
903 **Acknowledgements**
904 [We acknowledge funding support from the Bezos Earth Fund. We would like to thank Jack Warren for his valuable](#)
905 [efforts in analyzing point source emissions from MethaneAIR aerial campaigns.](#)

906
907 **Author contributions**
908 JPW and RG designed this study. JPW created the code used to produce all results, with inputs from MO, KM, DZA,
909 and AH. MethaneAIR analysis was provided by JB, MS, and SW. Multi-sensor airborne intercomparison was
910 performed by JPW and RG. JPW prepared the manuscript with input from all co-authors.

911
912 **Competing interests**
913 The authors declare that they have no conflict of interest.

914
915 **References**

916
917 Allen, D. T.: Methane emissions from natural gas production and use: reconciling bottom-up and top-down
918 measurements, *Current Opinion in Chemical Engineering*, 5, 78–83, <https://doi.org/10.1016/j.coche.2014.05.004>,
919 2014.

920 Alvarez, R. A., Zavala-Araiza, D., Lyon, D. R., Allen, D. T., Barkley, Z. R., Brandt, A. R., Davis, K. J., Herndon, S.
921 C., Jacob, D. J., Karion, A., Kort, E. A., Lamb, B. K., Lauvaux, T., Maasakkers, J. D., Marchese, A. J., Omara, M.,
922 Pacala, S. W., Peischl, J., Robinson, A. L., Shepson, P. B., Sweeney, C., Townsend-Small, A., Wofsy, S. C., and
923 Hamburg, S. P.: Assessment of methane emissions from the U.S. oil and gas supply chain, *Science*, 361, 186–188,
924 <https://doi.org/10.1126/science.aar7204>, 2018.

925 Enverus | Creating the future of energy together.: <https://www.enverus.com/>, last access: 25 March 2024.

926 Standards of Performance for New, Reconstructed, and Modified Sources and Emissions Guidelines for Existing
927 Sources: Oil and Natural Gas Sector Climate Review: [https://www.federalregister.gov/documents/2024/03/08/2024-
928 00366/standards-of-performance-for-new-reconstructed-and-modified-sources-and-emissions-guidelines-for](https://www.federalregister.gov/documents/2024/03/08/2024-00366/standards-of-performance-for-new-reconstructed-and-modified-sources-and-emissions-guidelines-for), last
929 access: 22 July 2024.

930 AR6 Synthesis Report: Climate Change 2023: <https://www.ipcc.ch/report/ar6/syr/>, last access: 6 March 2024.

931 MethaneAIR L4 Area Sources 2021 | Earth Engine Data Catalog: [https://developers.google.com/earth-
932 engine/datasets/catalog/EDF_MethaneSAT_MethaneAIR_methaneair-L4area-2021](https://developers.google.com/earth-engine/datasets/catalog/EDF_MethaneSAT_MethaneAIR_methaneair-L4area-2021), last access: 27 March 2024.

933 Brandt, A. R., Heath, G. A., and Cooley, D.: Methane Leaks from Natural Gas Systems Follow Extreme Distributions,
934 *Environ. Sci. Technol.*, 50, 12512–12520, <https://doi.org/10.1021/acs.est.6b04303>, 2016.

935 Brantley, H. L., Thoma, E. D., Squier, W. C., Guven, B. B., and Lyon, D.: Assessment of Methane Emissions from
936 Oil and Gas Production Pads using Mobile Measurements, *Environ. Sci. Technol.*, 48, 14508–14515,
937 <https://doi.org/10.1021/es503070q>, 2014.

938 Caulton, D. R., Lu, J. M., Lane, H. M., Buchholz, B., Fitts, J. P., Golston, L. M., Guo, X., Li, Q., McSpiritt, J., Pan,
939 D., Wendt, L., Bou-Zeid, E., and Zondlo, M. A.: Importance of Superemitter Natural Gas Well Pads in the Marcellus
940 Shale, *Environ. Sci. Technol.*, 53, 4747–4754, <https://doi.org/10.1021/acs.est.8b06965>, 2019.

941 Chan Miller, C., Roche, S., Wilzewski, J. S., Liu, X., Chance, K., Souri, A. H., Conway, E., Luo, B., Samra, J.,
942 Hawthorne, J., Sun, K., Staebell, C., Chulakadabba, A., Sargent, M., Benmergui, J. S., Franklin, J. E., Daube, B. C.,
943 Li, Y., Laughner, J. L., Baier, B. C., Gautam, R., Omara, M., and Wofsy, S. C.: Methane retrieval from MethaneAIR
944 using the CO₂ Proxy Approach: A demonstration for the upcoming MethaneSAT mission, *EGUsphere*, 1–40,
945 <https://doi.org/10.5194/egusphere-2023-1962>, 2023.

946 Chen, Y., Sherwin, E. D., Berman, E. S. F., Jones, B. B., Gordon, M. P., Wetherley, E. B., Kort, E. A., and Brandt, A.
947 R.: Quantifying Regional Methane Emissions in the New Mexico Permian Basin with a Comprehensive Aerial Survey,
948 *Environ. Sci. Technol.*, 56, 4317–4323, <https://doi.org/10.1021/acs.est.1c06458>, 2022.

949 [Chen, Y., Sherwin, E. D., Wetherley, E. B., Yakovlev, P. V., Berman, E. S. F., Jones, B. B., Hmiel, B., Lyon, D. R.,
950 Duren, R., Cusworth, D. H., and Brandt, A. R.: Reconciling ultra-emitter detections from two aerial hyperspectral
951 imaging surveys in the Permian Basin, 2024.](#)

952 Chulakadabba, A., Sargent, M., Lauvaux, T., Benmergui, J. S., Franklin, J. E., Chan Miller, C., Wilzewski, J. S.,
953 Roche, S., Conway, E., Souri, A. H., Sun, K., Luo, B., Hawthorne, J., Samra, J., Daube, B. C., Liu, X., Chance, K.,
954 Li, Y., Gautam, R., Omara, M., Rutherford, J. S., Sherwin, E. D., Brandt, A., and Wofsy, S. C.: Methane point source
955 quantification using MethaneAIR: a new airborne imaging spectrometer, *Atmospheric Measurement Techniques*, 16,
956 5771–5785, <https://doi.org/10.5194/amt-16-5771-2023>, 2023.

957 Cusworth, D. H., Thorpe, A. K., Ayase, A. K., Stepp, D., Heckler, J., Asner, G. P., Miller, C. E., Yadav, V., Chapman,
958 J. W., Eastwood, M. L., Green, R. O., Hmiel, B., Lyon, D. R., and Duren, R. M.: Strong methane point sources
959 contribute a disproportionate fraction of total emissions across multiple basins in the United States, *Proceedings of
960 the National Academy of Sciences*, 119, e2202338119, <https://doi.org/10.1073/pnas.2202338119>, 2022.

961 Deighton, J. A., Townsend-Small, A., Sturmer, S. J., Hoschouer, J., and Heldman, L.: Measurements show that
962 marginal wells are a disproportionate source of methane relative to production, *Journal of the Air & Waste
963 Management Association*, 70, 1030–1042, <https://doi.org/10.1080/10962247.2020.1808115>, 2020.

- 964 Duren, R. M., Thorpe, A. K., Foster, K. T., Rafiq, T., Hopkins, F. M., Yadav, V., Bue, B. D., Thompson, D. R.,
965 Conley, S., Colombi, N. K., Frankenberg, C., McCubbin, I. B., Eastwood, M. L., Falk, M., Herner, J. D., Croes, B. E.,
966 Green, R. O., and Miller, C. E.: California's methane super-emitters, *Nature*, 575, 180–184,
967 <https://doi.org/10.1038/s41586-019-1720-3>, 2019.
- 968 Elvidge, C. D., Zhizhin, M., Baugh, K., Hsu, F.-C., and Ghosh, T.: Methods for Global Survey of Natural Gas Flaring
969 from Visible Infrared Imaging Radiometer Suite Data, *Energies*, 9, 14, <https://doi.org/10.3390/en9010014>, 2015.
- 970 Fox, T. A., Barchyn, T. E., Risk, D., Ravikumar, A. P., and Hugenholtz, C. H.: A review of close-range and screening
971 technologies for mitigating fugitive methane emissions in upstream oil and gas, *Environ. Res. Lett.*, 14, 053002,
972 <https://doi.org/10.1088/1748-9326/ab0cc3>, 2019.
- 973 [Goetz, J. D., Floerchinger, C., Fortner, E. C., Wormhoudt, J., Massoli, P., Knighton, W. B., Herndon, S. C., Kolb, C.](#)
974 [E., Knipping, E., Shaw, S. L., and DeCarlo, P. F.: Atmospheric Emission Characterization of Marcellus Shale Natural](#)
975 [Gas Development Sites, *Environ. Sci. Technol.*, 49, 7012–7020, <https://doi.org/10.1021/acs.est.5b00452>, 2015.](#)
- 976 de Gouw, J. A., Veefkind, J. P., Roosenbrand, E., Dix, B., Lin, J. C., Landgraf, J., and Levelt, P. F.: Daily Satellite
977 Observations of Methane from Oil and Gas Production Regions in the United States, *Sci Rep*, 10, 1379,
978 <https://doi.org/10.1038/s41598-020-57678-4>, 2020.
- 979 Jacob, D. J., Varon, D. J., Cusworth, D. H., Dennison, P. E., Frankenberg, C., Gautam, R., Guanter, L., Kelley, J.,
980 McKeever, J., Ott, L. E., Poulter, B., Qu, Z., Thorpe, A. K., Worden, J. R., and Duren, R. M.: Quantifying methane
981 emissions from the global scale down to point sources using satellite observations of atmospheric methane,
982 *Atmospheric Chemistry and Physics*, 22, 9617–9646, <https://doi.org/10.5194/acp-22-9617-2022>, 2022.
- 983 Johnson, M. R., Tyner, D. R., and Szekeres, A. J.: Blinded evaluation of airborne methane source detection using
984 Bridger Photonics LiDAR, *Remote Sensing of Environment*, 259, 112418, <https://doi.org/10.1016/j.rse.2021.112418>,
985 2021.
- 986 Kunkel, W. M., Carre-Burritt, A. E., Aivazian, G. S., Snow, N. C., Harris, J. T., Mueller, T. S., Roos, P. A., and
987 Thorpe, M. J.: Extension of Methane Emission Rate Distribution for Permian Basin Oil and Gas Production
988 Infrastructure by Aerial LiDAR, *Environ. Sci. Technol.*, 57, 12234–12241, <https://doi.org/10.1021/acs.est.3c00229>,
989 2023.
- 990 Lan, X., Talbot, R., Laine, P., and Torres, A.: Characterizing Fugitive Methane Emissions in the Barnett Shale Area
991 Using a Mobile Laboratory, *Environ. Sci. Technol.*, 49, 8139–8146, <https://doi.org/10.1021/es5063055>, 2015.
- 992 Lu, X., Jacob, D. J., Wang, H., Maasackers, J. D., Zhang, Y., Scarpelli, T. R., Shen, L., Qu, Z., Sulprizio, M. P.,
993 Nesser, H., Bloom, A. A., Ma, S., Worden, J. R., Fan, S., Parker, R. J., Boesch, H., Gautam, R., Gordon, D., Moran,
994 M. D., Reuland, F., Villasana, C. A. O., and Andrews, A.: Methane emissions in the United States, Canada, and
995 Mexico: evaluation of national methane emission inventories and 2010–2017 sectoral trends by inverse analysis of in
996 situ (GLOBALVIEWplus CH₄ ObsPack) and satellite (GOSAT) atmospheric observations, *Atmospheric Chemistry*
997 *and Physics*, 22, 395–418, <https://doi.org/10.5194/acp-22-395-2022>, 2022.
- 998 Lu, X., Jacob, D. J., Zhang, Y., Shen, L., Sulprizio, M. P., Maasackers, J. D., Varon, D. J., Qu, Z., Chen, Z., Hmiel,
999 B., Parker, R. J., Boesch, H., Wang, H., He, C., and Fan, S.: Observation-derived 2010–2019 trends in methane
1000 emissions and intensities from US oil and gas fields tied to activity metrics, *Proceedings of the National Academy of*
1001 *Sciences*, 120, e2217900120, <https://doi.org/10.1073/pnas.2217900120>, 2023.
- 1002 Maasackers, J. D., Jacob, D. J., Sulprizio, M. P., Scarpelli, T. R., Nesser, H., Sheng, J., Zhang, Y., Lu, X., Bloom, A.
1003 A., Bowman, K. W., Worden, J. R., and Parker, R. J.: 2010–2015 North American methane emissions, sectoral
1004 contributions, and trends: a high-resolution inversion of GOSAT observations of atmospheric methane, *Atmospheric*
1005 *Chemistry and Physics*, 21, 4339–4356, <https://doi.org/10.5194/acp-21-4339-2021>, 2021.
- 1006 Miller, S. M., Wofsy, S. C., Michalak, A. M., Kort, E. A., Andrews, A. E., Biraud, S. C., Dlugokencky, E. J.,
1007 Eluszkiewicz, J., Fischer, M. L., Janssens-Maenhout, G., Miller, B. R., Miller, J. B., Montzka, S. A., Nehrkorn, T.,

- 1008 and Sweeney, C.: Anthropogenic emissions of methane in the United States, *Proceedings of the National Academy of*
1009 *Sciences*, 110, 20018–20022, <https://doi.org/10.1073/pnas.1314392110>, 2013.
- 1010 Mitchell, A. L., Tkacik, D. S., Roscioli, J. R., Herndon, S. C., Yacovitch, T. I., Martinez, D. M., Vaughn, T. L.,
1011 Williams, L. L., Sullivan, M. R., Floerchinger, C., Omara, M., Subramanian, R., Zimmerle, D., Marchese, A. J., and
1012 Robinson, A. L.: Measurements of Methane Emissions from Natural Gas Gathering Facilities and Processing Plants:
1013 Measurement Results, *Environ. Sci. Technol.*, 49, 3219–3227, <https://doi.org/10.1021/es5052809>, 2015.
- 1014 Nesser, H., Jacob, D. J., Maasackers, J. D., Lorente, A., Chen, Z., Lu, X., Shen, L., Qu, Z., Sulprizio, M. P., Winter,
1015 M., Ma, S., Bloom, A. A., Worden, J. R., Stavins, R. N., and Randles, C. A.: High-resolution U.S. methane emissions
1016 inferred from an inversion of 2019 TROPOMI satellite data: contributions from individual states, urban areas, and
1017 landfills, *EGUosphere*, 1–36, <https://doi.org/10.5194/egusphere-2023-946>, 2023.
- 1018 Ocko, I. B., Sun, T., Shindell, D., Oppenheimer, M., Hristov, A. N., Pacala, S. W., Mauzerall, D. L., Xu, Y., and
1019 Hamburg, S. P.: Acting rapidly to deploy readily available methane mitigation measures by sector can immediately
1020 slow global warming, *Environ. Res. Lett.*, 16, 054042, <https://doi.org/10.1088/1748-9326/abf9c8>, 2021.
- 1021 Omara, M., Sullivan, M. R., Li, X., Subramanian, R., Robinson, A. L., and Presto, A. A.: Methane Emissions from
1022 Conventional and Unconventional Natural Gas Production Sites in the Marcellus Shale Basin, *Environ. Sci. Technol.*,
1023 50, 2099–2107, <https://doi.org/10.1021/acs.est.5b05503>, 2016.
- 1024 Omara, M., Zimmerman, N., Sullivan, M. R., Li, X., Ellis, A., Cesa, R., Subramanian, R., Presto, A. A., and Robinson,
1025 A. L.: Methane Emissions from Natural Gas Production Sites in the United States: Data Synthesis and National
1026 Estimate, *Environ. Sci. Technol.*, 52, 12915–12925, <https://doi.org/10.1021/acs.est.8b03535>, 2018.
- 1027 Omara, M., Zavala-Araiza, D., Lyon, D. R., Hmiel, B., Roberts, K. A., and Hamburg, S. P.: Methane emissions from
1028 US low production oil and natural gas well sites, *Nat Commun*, 13, 2085, [https://doi.org/10.1038/s41467-022-29709-](https://doi.org/10.1038/s41467-022-29709-3)
1029 3, 2022.
- 1030 Omara, M., Himmelberger, A., MacKay, K., Williams, J. P., Benmergui, J., Sargent, M., Wofsy, S. C., and Gautam,
1031 R.: Constructing a measurement-based spatially explicit inventory of US oil and gas methane emissions, *Earth System*
1032 *Science Data Discussions*, 1–25, <https://doi.org/10.5194/essd-2024-72>, 2024.
- 1033 Plant, G., Kort, E. A., Brandt, A. R., Chen, Y., Fordice, G., Gorchoy Negron, A. M., Schwietzke, S., Smith, M., and
1034 Zavala-Araiza, D.: Inefficient and unlit natural gas flares both emit large quantities of methane, *Science*, 377, 1566–
1035 1571, <https://doi.org/10.1126/science.abq0385>, 2022.
- 1036 Ravikumar, A. P., Wang, J., McGuire, M., Bell, C. S., Zimmerle, D., and Brandt, A. R.: “Good versus Good Enough?”
1037 Empirical Tests of Methane Leak Detection Sensitivity of a Commercial Infrared Camera, *Environ. Sci. Technol.*, 52,
1038 2368–2374, <https://doi.org/10.1021/acs.est.7b04945>, 2018.
- 1039 Rella, C. W., Hoffnagle, J., He, Y., and Tajima, S.: Local- and regional-scale measurements of CH₄, δ¹³CH₄, and C₂H₆
1040 in the Uintah Basin using a mobile stable isotope analyzer, *Atmospheric Measurement Techniques*, 8, 4539–4559,
1041 <https://doi.org/10.5194/amt-8-4539-2015>, 2015.
- 1042 Riddick, S. N., Mauzerall, D. L., Celia, M. A., Kang, M., Bressler, K., Chu, C., and Gum, C. D.: Measuring methane
1043 emissions from abandoned and active oil and gas wells in West Virginia, *Science of The Total Environment*, 651,
1044 1849–1856, <https://doi.org/10.1016/j.scitotenv.2018.10.082>, 2019.
- 1045 Riddick, S. N., Ancona, R., Mbua, M., Bell, C. S., Duggan, A., Vaughn, T. L., Bennett, K., and Zimmerle, D. J.: A
1046 quantitative comparison of methods used to measure smaller methane emissions typically observed from
1047 superannuated oil and gas infrastructure, *Atmospheric Measurement Techniques*, 15, 6285–6296,
1048 <https://doi.org/10.5194/amt-15-6285-2022>, 2022.
- 1049 Riddick, S. N., Mbua, M., Santos, A., Emerson, E. W., Cheptonui, F., Houlihan, C., Hodshire, A. L., Anand, A.,
1050 Hartzell, W., and Zimmerle, D. J.: Methane emissions from abandoned oil and gas wells in Colorado, *Science of The*
1051 *Total Environment*, 922, 170990, <https://doi.org/10.1016/j.scitotenv.2024.170990>, 2024.

- 1052 Robertson, A. M., Edie, R., Snare, D., Soltis, J., Field, R. A., Burkhart, M. D., Bell, C. S., Zimmerle, D., and Murphy,
1053 S. M.: Variation in Methane Emission Rates from Well Pads in Four Oil and Gas Basins with Contrasting Production
1054 Volumes and Compositions, *Environ. Sci. Technol.*, 51, 8832–8840, <https://doi.org/10.1021/acs.est.7b00571>, 2017.
- 1055 Robertson, A. M., Edie, R., Field, R. A., Lyon, D., McVay, R., Omara, M., Zavala-Araiza, D., and Murphy, S. M.:
1056 New Mexico Permian Basin Measured Well Pad Methane Emissions Are a Factor of 5–9 Times Higher Than U.S.
1057 EPA Estimates, *Environ. Sci. Technol.*, 54, 13926–13934, <https://doi.org/10.1021/acs.est.0c02927>, 2020.
- 1058 Rutherford, J. S., Sherwin, E. D., Ravikumar, A. P., Heath, G. A., Englander, J., Cooley, D., Lyon, D., Omara, M.,
1059 Langfitt, Q., and Brandt, A. R.: Closing the methane gap in US oil and natural gas production emissions inventories,
1060 *Nat Commun.*, 12, 4715, <https://doi.org/10.1038/s41467-021-25017-4>, 2021.
- 1061 Shen, L., Gautam, R., Omara, M., Zavala-Araiza, D., Maasackers, J. D., Scarpelli, T. R., Lorente, A., Lyon, D., Sheng,
1062 J., Varon, D. J., Nesser, H., Qu, Z., Lu, X., Sulprizio, M. P., Hamburg, S. P., and Jacob, D. J.: Satellite quantification
1063 of oil and natural gas methane emissions in the US and Canada including contributions from individual basins,
1064 *Atmospheric Chemistry and Physics*, 22, 11203–11215, <https://doi.org/10.5194/acp-22-11203-2022>, 2022.
- 1065 Sherwin, E., Zhang, Z., Chen, Y., Wetherley, E. B., Yakovlev, P., Berman, E. S. F., Jones, B. B., Thorpe, A. K.,
1066 Ayasse, A. K., Duren, R., Brandt, A. R., and Cusworth, D. H.: Quantifying oil and natural gas system emissions using
1067 one million aerial site measurements, <https://doi.org/10.21203/rs.3.rs-2406848/v1>, 2023a.
- 1068 Sherwin, E. D., Rutherford, J. S., Chen, Y., Aminfard, S., Kort, E. A., Jackson, R. B., and Brandt, A. R.: Single-blind
1069 validation of space-based point-source detection and quantification of onshore methane emissions, *Sci Rep.*, 13, 3836,
1070 <https://doi.org/10.1038/s41598-023-30761-2>, 2023b.
- 1071 Sherwin, E. D., Rutherford, J. S., Zhang, Z., Chen, Y., Wetherley, E. B., Yakovlev, P. V., Berman, E. S. F., Jones, B.
1072 B., Cusworth, D. H., Thorpe, A. K., Ayasse, A. K., Duren, R. M., and Brandt, A. R.: US oil and gas system emissions
1073 from nearly one million aerial site measurements, *Nature*, 627, 328–334, <https://doi.org/10.1038/s41586-024-07117-5>, 2024.
- 1075 Stavropoulou, F., Vinković, K., Kers, B., de Vries, M., van Heuven, S., Korbeň, P., Schmidt, M., Wietzel, J., Jagoda,
1076 P., Necki, J. M., Bartyzel, J., Maazallahi, H., Menoud, M., van der Veen, C., Walter, S., Tuzson, B., Ravelid, J.,
1077 Morales, R. P., Emmenegger, L., Brunner, D., Steiner, M., Hensen, A., Velzeboer, I., van den Bulk, P., Denier van
1078 der Gon, H., Delre, A., Edjabou, M. E., Scheutz, C., Corbu, M., Iancu, S., Moaca, D., Scarlat, A., Tudor, A., Vizireanu,
1079 I., Calcan, A., Ardelean, M., Ghemulet, S., Pana, A., Constantinescu, A., Cusa, L., Nica, A., Baciu, C., Pop, C.,
1080 Radovici, A., Mereuta, A., Stefanie, H., Dandocsi, A., Hermans, B., Schwietzke, S., Zavala-Araiza, D., Chen, H., and
1081 Röckmann, T.: High potential for CH₄ emission mitigation from oil infrastructure in one of EU's major production
1082 regions, *Atmospheric Chemistry and Physics*, 23, 10399–10412, <https://doi.org/10.5194/acp-23-10399-2023>, 2023.
- 1083 Thorpe, M. J., Krietinger, A., Altamura, D., Dudiak, C. D., Conrad, B. M., Tyner, D. R., Johnson, M. R., Brasseur, J.
1084 K., Roos, P., Kunkel, W., Carre-Burritt, A., Abate, J., Price, T., Yaralian, D., Kennedy, B., Newton, E., Rodriguez,
1085 E., Elfar, O. I., and Zimmerle, D. J.: Deployment-invariant probability of detection characterization for aerial LiDAR
1086 methane detection, 2024.
- 1087 Tyner, D. R. and Johnson, M. R.: Where the Methane Is—Insights from Novel Airborne LiDAR Measurements
1088 Combined with Ground Survey Data, *Environ. Sci. Technol.*, 55, 9773–9783, <https://doi.org/10.1021/acs.est.1c01572>,
1089 2021.
- 1090 Inventory of U.S. Greenhouse Gas Emissions and Sinks: [https://www.epa.gov/ghgemissions/inventory-us-](https://www.epa.gov/ghgemissions/inventory-us-greenhouse-gas-emissions-and-sinks)
1091 [greenhouse-gas-emissions-and-sinks](https://www.epa.gov/ghgemissions/inventory-us-greenhouse-gas-emissions-and-sinks), last access: 6 March 2024.
- 1092 EPA's Final Rule for Oil and Natural Gas Operations Will Sharply Reduce Methane and Other Harmful Pollution.:
1093 <https://www.epa.gov/controlling-air-pollution-oil-and-natural-gas-operations/epas-final-rule-oil-and-natural-gas>, last
1094 access: 5 March 2024.

- 1095 Weller, Z. D., Hamburg, S. P., and von Fischer, J. C.: A National Estimate of Methane Leakage from Pipeline Mains
1096 in Natural Gas Local Distribution Systems, *Environ. Sci. Technol.*, 54, 8958–8967,
1097 <https://doi.org/10.1021/acs.est.0c00437>, 2020.
- 1098 Williams, J. P., Regehr, A., and Kang, M.: Methane Emissions from Abandoned Oil and Gas Wells in Canada and the
1099 United States, *Environ. Sci. Technol.*, 55, 563–570, <https://doi.org/10.1021/acs.est.0c04265>, 2021.
- 1100 Williams, J. P., El Hachem, K., and Kang, M.: Controlled-release testing of the static chamber methodology for direct
1101 measurements of methane emissions, *Atmospheric Measurement Techniques*, 16, 3421–3435,
1102 <https://doi.org/10.5194/amt-16-3421-2023>, 2023.
- 1103 Worden, J. R., Cusworth, D. H., Qu, Z., Yin, Y., Zhang, Y., Bloom, A. A., Ma, S., Byrne, B. K., Scarpelli, T.,
1104 Maasackers, J. D., Crisp, D., Duren, R., and Jacob, D. J.: The 2019 methane budget and uncertainties at 1° resolution
1105 and each country through Bayesian integration Of GOSAT total column methane data and a priori inventory estimates,
1106 *Atmospheric Chemistry and Physics*, 22, 6811–6841, <https://doi.org/10.5194/acp-22-6811-2022>, 2022.
- 1107 Xia, H., Strayer, A., and Ravikumar, A. P.: The Role of Emission Size Distribution on the Efficacy of New
1108 Technologies to Reduce Methane Emissions from the Oil and Gas Sector, *Environ. Sci. Technol.*, 58, 1088–1096,
1109 <https://doi.org/10.1021/acs.est.3c05245>, 2024.
- 1110 Yacovitch, T. I., Herndon, S. C., Pétron, G., Kofler, J., Lyon, D., Zahniser, M. S., and Kolb, C. E.: Mobile Laboratory
1111 Observations of Methane Emissions in the Barnett Shale Region, *Environ. Sci. Technol.*, 49, 7889–7895,
1112 <https://doi.org/10.1021/es506352j>, 2015.
- 1113 Zhang, Y., Gautam, R., Pandey, S., Omara, M., Maasackers, J. D., Sadavarte, P., Lyon, D., Nesser, H., Sulprizio, M.
1114 P., Varon, D. J., Zhang, R., Houweling, S., Zavala-Araiza, D., Alvarez, R. A., Lorente, A., Hamburg, S. P., Aben, I.,
1115 and Jacob, D. J.: Quantifying methane emissions from the largest oil-producing basin in the United States from space,
1116 *Science Advances*, 6, eaaz5120, <https://doi.org/10.1126/sciadv.aaz5120>, 2020.
- 1117 Zhou, X., Yoon, S., Mara, S., Falk, M., Kuwayama, T., Tran, T., Cheadle, L., Nyarady, J., Croes, B., Scheehle, E.,
1118 Herner, J. D., and Vijayan, A.: Mobile sampling of methane emissions from natural gas well pads in California,
1119 *Atmospheric Environment*, 244, 117930, <https://doi.org/10.1016/j.atmosenv.2020.117930>, 2021.
- 1120 Zimmerle, D., Vaughn, T., Luck, B., Lauderdale, T., Keen, K., Harrison, M., Marchese, A., Williams, L., and Allen,
1121 D.: Methane Emissions from Gathering Compressor Stations in the U.S., *Environ. Sci. Technol.*, 54, 7552–7561,
1122 <https://doi.org/10.1021/acs.est.0c00516>, 2020.

1123

1124

1125

1126

1127

1128

1129

1130